Protein disulfide isomerases are promising targets for predicting the survival and tumor progression in glioma patients

Zhigang Peng[1,*], Yu Chen[2,*], Hui Cao[3], Hecun Zou[4], Xin Wan[1], Wenjing Zeng[4], Yanling Liu[4], Jiaqing Hu[5], Nan Zhang[6], Zhiwei Xia[7], Zhixiong Liu[1], Quan Cheng[1,4,8]

[1]Department of Neurosurgery, Xiangya Hospital, Central South University, Changsha 410008, Hunan, P. R. China
[2]Department of Neurosurgery, The First Affiliated Hospital of Zhengzhou University, Zhengzhou 450001, Henan, P. R. China
[3]Department of Psychiatry, The Second People's Hospital of Hunan Province, The Affiliated Hospital of Hunan University of Chinese Medicine, Changsha 410007, Hunan, P. R. China
[4]Department of Clinical Pharmacology, Xiangya Hospital, Central South University, Changsha 410008, Hunan, P. R. China
[5]Department of Emergency, The Second People's Hospital of Hunan Province, The Affiliated Hospital of Hunan University of Chinese Medicine, Changsha 410007, Hunan, P. R. China
[6]School of Bioinformatics Science and Technology, Harbin Medical University, Harbin 150081, Heilongjiang, P. R. China
[7]Department of Neurology, Xiangya Hospital, Central South University, Changsha 410008, Hunan, P. R. China
[8]Institute of Clinical Pharmacology, Central South University; Hunan Key Laboratory of Pharmacogenetics, Changsha 410078, Hunan, P. R. China
*Equal contribution

Correspondence to: Quan Cheng, Zhixiong Liu; **email:** chengquan@csu.edu.cn, zhixiongliu@csu.edu.cn
Keywords: PDI family, PDI, GBM, glioma, prognosis
Received: September 13, 2019   **Accepted:** January 7, 2020   **Published:** February 5, 2020

ABSTRACT

The present study focused on the expression patterns, prognostic values and potential mechanism of the PDI family in gliomas. Most PDI family members' mRNA expressions were observed significantly different between gliomas classified by clinical features. Construction of the PDI signature, cluster and risk score models of glioma was done using GSVA, consensus clustering analysis, and LASSO Cox regression analysis respectively. High values of PDI signature/ risk score and cluster 1 in gliomas were associated with malignant clinicopathological characteristics and poor prognosis. Analysis of the distinctive genomic alterations in gliomas revealed that many cases having high PDI signature and risk score were associated with genomic aberrations of driver oncogenes. GSVA analysis showed that PDI family was involved in many signaling pathways in ERAD, apoptosis, and MHC class I among many more. Prognostic nomogram revealed that the risk score was a good prognosis indicator for gliomas. The qRT-PCR and immunohistochemistry confirmed that P4HB, PDIA4 and PDIA5 were overexpressed in gliomas. In summary, this research highlighted the clinical importance of PDI family in tumorigenesis and progression in gliomas.

INTRODUCTION

Gliomas are the most common brain and central nervous system (CNS) tumors. According to cancer statistics, gliomas account for approximately 80% of all malignant primary brain tumors and 57.3% of gliomas was glioblastoma (GBM) [1, 2]. Hideo Nakamura et al. reported that the incidence rate for glioma was 6·6 per

100,000 and nearly half of this was glioblastoma [3]. Of note, the Central Brain Tumor Registry of the United States (CBTRUS) statistical report revealed that the incidence rate of glioblastoma increased with age, with 1.24 per 100,000 population in age 35–44 years, 8.07 in age 55–64 years, 12.98 in age 65–74 years and with the highest rates in 75–84 years (15.29 per 100,000 population) [2]. According to WHO classification, GBM, is defined as a grade IV glioma with its molecular classification revealing four subtypes; proneural, neural, classical, and mesenchymal [4, 5]. After a safe surgical resection, GBM patients are treated with radiotherapy and chemotherapy [6]. Unfortunately, their survival rate is very limited with most of the patients dying within 15–18 months post-diagnosis while just 6.8% of the patients survive up to five years [2, 7–9]. Consequently, glioblastoma is a major threat to human health, especially in the elderly.

Protein disulfide isomerase (PDI) family consists of twenty-one members sharing a common structure (the TRX-like domain). Their proteins have an N-terminal signal peptide consisting of 15–30 amino acids which are cleaved upon entry into the endoplasmic reticulum [10]. The PDI family members are mainly located in the ER, with a few also found in other cellular compartments, including the cell surface, cytosol, mitochondria, and nucleus [11]. This PDI family of enzymes have been identified primarily as reductases, oxidases, isomerases, and enzymatic chaperones catalyzing disulfide bond formation, breakage, rearrangement, and oxidative protein folding [11].

Several studies have linked protein disulfide isomerases (PDIs) to the regulation of proliferation, invasion, and metastasis of various cancers, such as brain, lymphoma, kidney, ovarian, prostate, and lung cancers [12]. PDIA6 was found to be over-expressed in bladder cancer (BC) where it facilitated proliferation and invasion in BC cells via Wnt/β-catenin signaling pathway [13]. Moreover, P4HB, PDIA3, and PDIA4 were found to be up-regulated in ovarian cancer and associated with the tumor grade and poor prognosis [14]. PDIA1 and PDIA3 serve vital roles in the progression of diffuse glioma. P4HB function using bacitracin attenuated the phosphorylated FAK and the secreted MMP-2, the downstream molecules of integrin, restrained migration of U87-MG Glioma cells [15]. Other studies have revealed that PDIs inhibition suppresses the growth of tumors. Inhibition of PDIA1 was shown to decrease the resistance to temozolomide (TMZ) in malignant glioma [16, 17]. Recently, Horibe et al. suggested that PDIA5 knockdown in GBM cells significantly suppressed the growth and migration of tumor cells [18].

PDIs have been associated with the progression of GBM, however little is known on the relationship between PDIs expression and the clinical outcome in gliomas. In the present study, the aim was to conduct a comprehensive analysis of twenty-one PDI family members. Bioinformatic tools and qRT-PCR were used for mRNA expression in gliomas. Therefore, data obtained revealed several new potential signaling pathways of PDIs involved in glioma progression. Furthermore, a prognostic nomogram using PDIs-based survival risk score and other clinical factors was established, and these provided novel insights for future diagnostics and therapeutic targets of glioma.

RESULTS

The relationship between PDIs mRNA expression and clinicopathological characteristics of glioma

In humans, twenty-one members of the PDI family have been identified. In this study, TCGA and CGGA databases data revealed the correlation between PDIs mRNA expression and clinical-pathological features in gliomas. High transcription levels of P4HB, PDIA3, PDIA4, PDIA5, PDIA6, ERP27, ERP29, ERP44, TMX1, TMX3, TXNDC5, TXNDC12, AGR3, and DNAJC10 were found in GBM tissues. However, the transcription levels of PDIA2, AGR2, CASQ1, and CASQ2 were lower in GBM tissues than in LGG tissues (Figure 1A–1F). There was no significant difference in the mRNA level of PDILT between GBM and LGG samples based on both TCGA and CGGA (Figure 1A–1F). However, there were inconsistent findings on the mRNA expression levels of TMX2 and TMX4 from TCGA and CGGA datasets in GBM versus in LGG tissues (Figure 1A–1F). Furthermore, TCGA and CGGA datasets confirmed the significant correlation between WHO grades and mRNA levels of P4HB, PDIA3, PDIA4, PDIA5, PDIA6, ERP27, ERP29, ERP44, TMX1, TMX3, TXNDC12, DNAJC10, and CASQ1 (Figure 1B–1G). In the TCGA LGGGBM cohort, the mRNA expression of P4HB, PDIA3, PDIA4, PDIA5, PDIA6, ERP27, ERP29, ERP44, TMX1, TMX3, TMX4, TXNDC5, TXNDC12, AGR3, and DNAJC10 in gliomas with mutant IDH were lower in comparison to those in gliomas with wild-type IDH. The mRNA expression of PDIA2, CASQ1, and CASQ2 was higher in the mutant IDH group (Figure 1C). There was no significant difference in the expression levels of PDILT, TMX2, and AGR2 between the two groups. Unlike previous findings, within the CGGA LGGGBM cohort, TMX2 was up-regulated in gliomas with mutant IDH and the expression of TMX4 in the two groups was not statistically significant (Figure 1H). There was a significant difference in the expression of some members of the PDI family between the two groups

(mutant IDH vs. wildtype IDH) in the LGG and GBM cohort (Figure 1D, 1I, Supplementary Figure 1A, 1B). Further, PDIA2, TMX2, and CASQ1 were down-regulated in LGG with mutant IDH and 1p19q noncodeletion, and PDIA5, PDILT, ERP27, TMX1, TXNDC12, AGR3, and DNAJC10 were up-regulated in both TCGA and CGGA (Figure 1E, Supplementary Figure 1C). There was no significant difference in the mRNA level of other members of the PDI gene family in the low-grade gliomas with mutant IDH (1p19q codeletion vs. 1p19q noncodeletion) in TCGA or CGGA (Figure 1E, Supplementary Figure 1C).
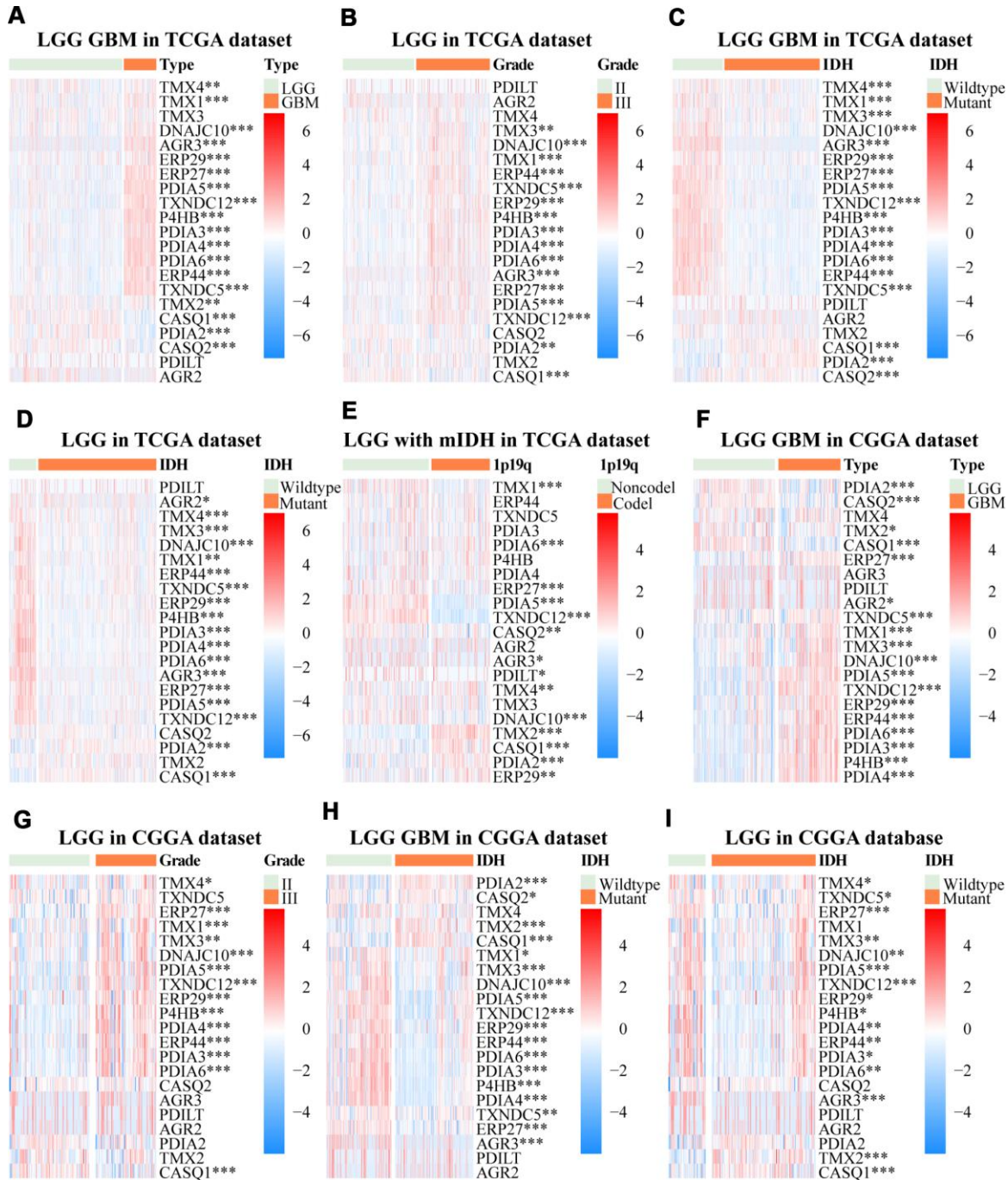

Figure 1. Relationship between mRNA expression patterns of PDIs in gliomas with different clinical characteristics (cancer type, WHO grade, the status of IDH and 1p19q). The heat maps, based on the public data from TCGA and CGGA databases, demonstrated upregulated mRNA (red) or downregulated mRNA (blue) of the PDI family members in the subgroups. TCGA database as training set and CGGA database as the validation set. * $p < 0.05$, ** $p < 0.01$, *** $p < 0.001$.

Construction of the PDI signature model

To construct a PDIs-based signature model for both in training and validation groups GSVA was performed. Heat maps presented the expression profiles of PDI family members ranked according to their PDI signatures from the TCGA and CGGA datasets (Figure 2A, 2B). In the TCGA database, gliomas were classified into four molecular subtypes; proneural (PN), neural (NE), classical (CL), and mesenchymal (ME). In the current study, gliomas were further classified into two main subtypes based on their malignancy (CL+ME vs. NE+PN). The value of PDI signature in patients separated by subtype, MGMT promoter status, 1p19q codel status, IDH status, gender, age, grade, and cancer (LGG vs. GBM). In the TCGA LGGGBM cohort there were significant differences between the patients separated by subtype (CL+ME vs. NE+PN), MGMT promoter status, 1p19q codel status, IDH status, age, grade, cancer (LGG vs. GBM), but not by gender (Figure 2C–2J). Supplementary Figure 1D showed that there was no significant difference in PDI signature between classical and mesenchymal subtypes. Further, there were statistical differences observed in the groups divided by subtype (CL+ME vs. NE+PN), 1p19q codel status, IDH status in TCGA LGG and/or GBM cohort. However, there was no significant difference in the MGMT promoter status and IDH status in the TCGA GBM cohort (Supplementary Figure 1E–1J).

The patients were divided into two groups (high vs. low group) using the median value of PDI signature as the cut-off value to investigate the relationship between the value of PDI signature and patients' prognosis. In the TCGA LGGGBM cohort, the Kaplan–Meier plot revealed that the high value of PDI signature was associated with poor OS, PFI and DSS (Supplementary Figure 2A–2C). Similar findings were also found in LGG and GBM (Supplementary Figure 2D–2I). Furthermore, as validated in the CGGA datasets, patients in the low-value group exhibited longer OS than those in the the high-value group (Supplementary Figure 2J–2L). These findings indicated a significant association between PDI signature and clinical features and the high value of PDI signature was associated with poor prognosis.

As previously described, somatic mutations and copy number variations in the two groups were analyzed (1st vs. 4th). High mutation frequency in IDH1, TP53, and ATRX were associated with low PDI signature in gliomas (IDH1, 89% vs. 17%; TP53, 48% vs. 31%; ATRX, 32% vs. 15%), whereas TTN, MUC16, and PIK3CA were associated with high PDI signature (TTN, 10% vs. 24%; MUC16, 8% vs. 13%; PIK3CA, 5% vs. 11%) (Figure 3A–3B). The mutation frequency of CIC in the low PDI signature group reached 20% (Figure 3A) while the mutations in PTEN,

EGFR, NF1, and RYR2 were enriched in the cases with high PDI signature, of which all their frequencies were more than 10% (Figure 3B).

GSVA was performed to characterize the potential function of PDIs in gliomas. Most of the functional pathways were enriched in higher PDI signature group. Some important biological processes in which PDI was known to be involved were identified, such as unfolded protein response (UPR), endoplasmic reticulum-associated degradation (ERAD), endoplasmic reticulum stress (ERS). Many pathways were also associated with cancer pathogenesis, invasion, and metastasis, including WNT signaling pathways, positive regulation of NF kappa B transcription factor activity, vascular endothelial growth factor receptor (VEGFR) signaling pathway, apoptotic signaling pathway, regulation of MAPK cascade, cell cycle, p53 signaling pathway, cytosolic DNA sensing, pathways in cancer, and JAK-STAT signaling pathway. There were also immune-related regulatory pathways identified which did not traditionally focus on PDIs such as antigen processing and presentation, chemokine signaling pathway, B cell receptor signaling pathway, T cell receptor signaling pathway, and natural killer cell-mediated cytotoxicity (Figure 3C).

Constructing the cluster model of glioma based on consensus clustering analysis

Tumor samples from TCGA and CGGA datasets were grouped into two clusters (cluster 1, cluster 2) using consensus clustering analysis to explore PDIs' potential predictive and prognostic value. Cumulative distribution function (CDF) curves and consensus matrixes (Supplementary Figure 3A–3D) determined the optimal number of clusters (k=2). As shown in Figure 4A–4B, cluster 1 was related to the status of MGMT promoter unmethylated, 1p19q noncodel, IDH wildtype, higher grade, and GBM. Glioma patients in cluster 1 also had a higher PDI signature compared with cluster 2. The principal component analysis demonstrated the difference of PDIs mRNA expression between the two clusters (Figure 4C–4D).

Apart from differences in clinical characteristics between cluster 1 and cluster 2, there were also differences in prognosis in the two groups. In the TCGA datasets, Cluster 2 significantly correlated with longer OS, PFI and DSS in contrast to cluster 1 (Figure 4E–4G).

Constructing the risk score model based on least absolute shrinkage and selection operator (LASSO) Cox regression analysis

A total of 18 significant factors with $p < 0.05$ were selected through the univariate COX regression analysis
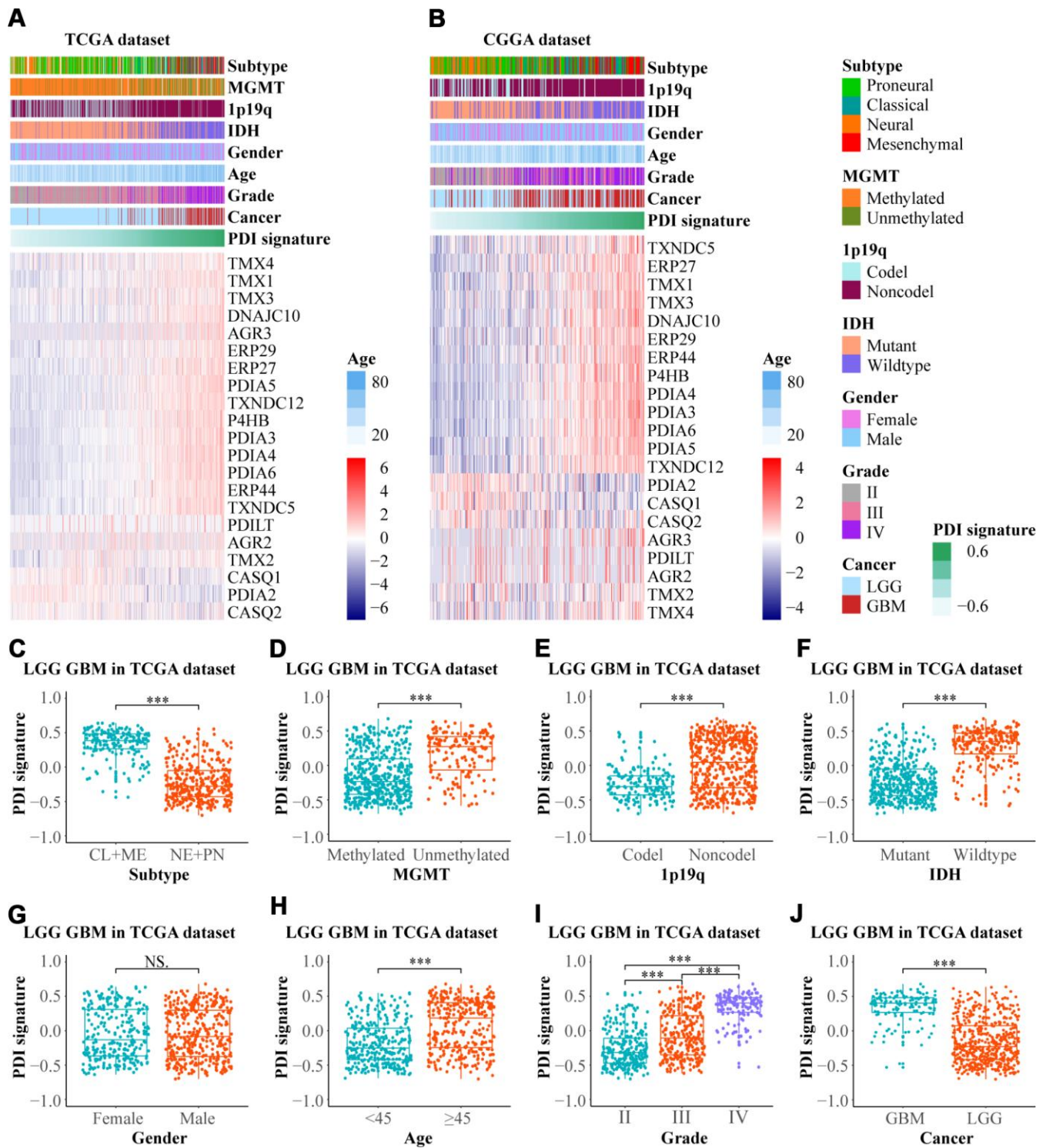
Figure 2. The relationship between the PDI signature and clinical features in gliomas. Heat maps revealed the expression profiles of PDIs and the distribution of clinicopathological features in gliomas based on data from TCGA (**A**) and CGGA (**B**) in which the samples were ranked according to their PDI signature. In the TCGA dataset, the distribution of PDI signature in the subgroups classified by subtype (**C**) MGMT promoter status (**D**) 1p19q codel status (**E**) IDH status (**F**) gender (**G**) age (**H**) grade (**I**) and cancer (**J**). TCGA database as training set and CGGA database as the validation set. *** $p < 0.001$, NS. $p > 0.05$.
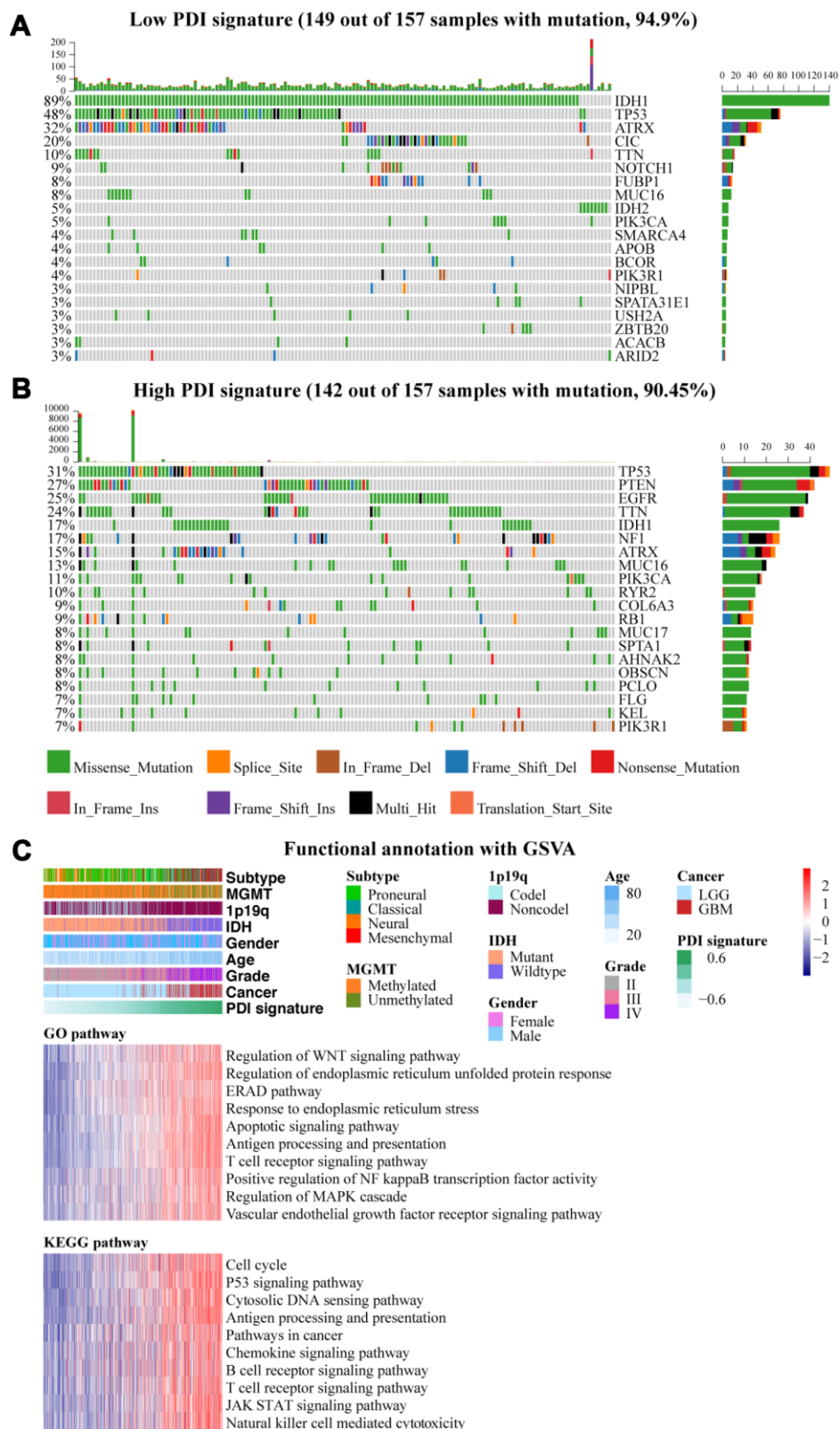
Figure 3. (**A**, **B**) Genetic alteration profiles associated with PDI signature in TCGA and CGGA datasets. Oncoprint depicts the distribution of the top 20 genes with the highest mutation frequency in each glioma group (low PDI signature vs high PDI signature). (**C**) Functional annotation of PDI gene family with PDI signature, including GO and KEGG. The upper one panel shows the distribution of PDI signature and clinical features, and the lower two panels show the gene set enrichment in different pathways analyzed by GSVA package of R. TCGA database as training set and CGGA database as the validation set.

(P4HB, PDIA2, PDIA3, PDIA4, PDIA5, PDIA6, ERP27, ERP29, ERP44, TMX1, TMX3, TMX4, TXNDC5, TXNDC12, AGR3, DNAJC10, CASQ1, CASQ2) (Figure 5A–5B). These were then introduced into the LASSO Cox regression model, which exhibited the five most meaningful PDI family members and their coefficients which was used to calculate the risk score (Figure 5C–5E). The heat maps displayed the expression profiles of PDIs both in TCGA and CGGA datasets, as the samples were ranked according to their risk scores (Figure 6A, 6B). In the TCGA LGGGBM dataset, the risk score in different groups was stratified by clinical features, and exhibited by box plots. The higher risk score was related to the subtype (CL+ME vs. NE+PN), MGMT promoter unmethylated, 1p19q noncodel, IDH wildtype, age≥45, and GBM groups
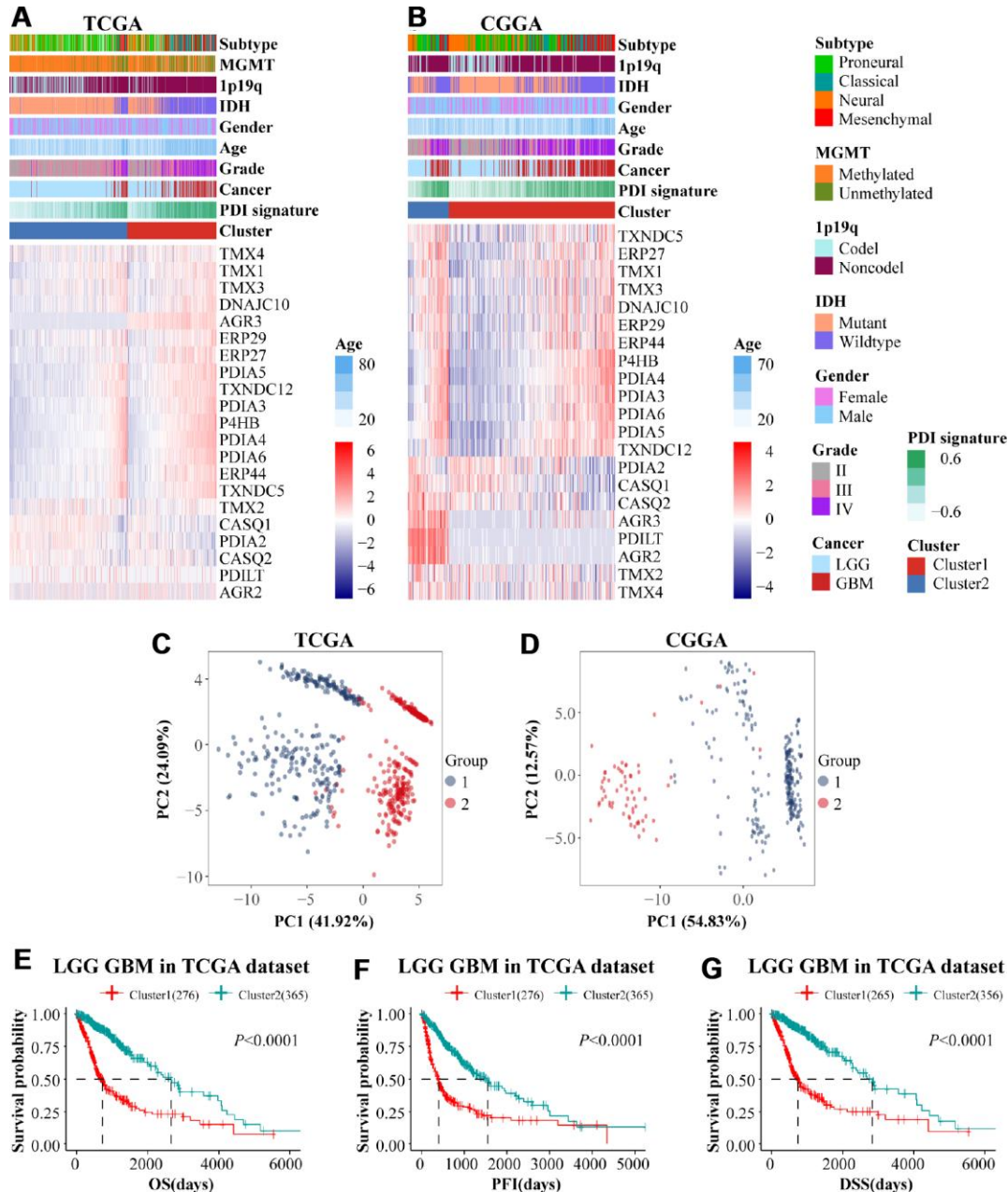

Figure 4. (**A**, **B**) Comparison of the expression levels of PDIs and clinical features between two subgroups (cluster 1 vs cluster 2). Principal component analysis (PCA) was performed to reveal the difference of PDIs mRNA expression between two clusters in TCGA (**C**) and CGGA (**D**). The prognostic value of clusters in glioma patients. Kaplan–Meier survival analyses were used to demonstrate differences in OS, PFI and DSS between the two clusters of LGGGBM samples from TCGA (**E**–**G**) and CGGA (**H**). TCGA database as training set and CGGA database as the validation set.

(Figure 6C–6F, 6H, 6J, 6E). As shown in Supplementary Figure 3E, there was no significant difference in the risk score between classical and mesenchymal subtypes. Moreover, the risk score increased along with the WHO grade of gliomas (Figure 6I). However, there was no significant difference in groups separated by gender (Figure 6G). There were statistical differences in the LGG/GBM patients classified by subtype (CL+ME vs. NE+PN), 1p19q codel status, IDH status, but not by

MGMT promoter status in the TCGA GBM cohort (Supplementary Figure 3F–3K).

The prognostic differences between low and high-risk groups divided by the median risk score were compared. As shown in Supplementary Figure 4A–4I, the patients with high-risk score had significantly shorter OS, PFI, and DSS than those with a low-risk score in the TCGA LGGGBM, LGG, GBM cohorts.
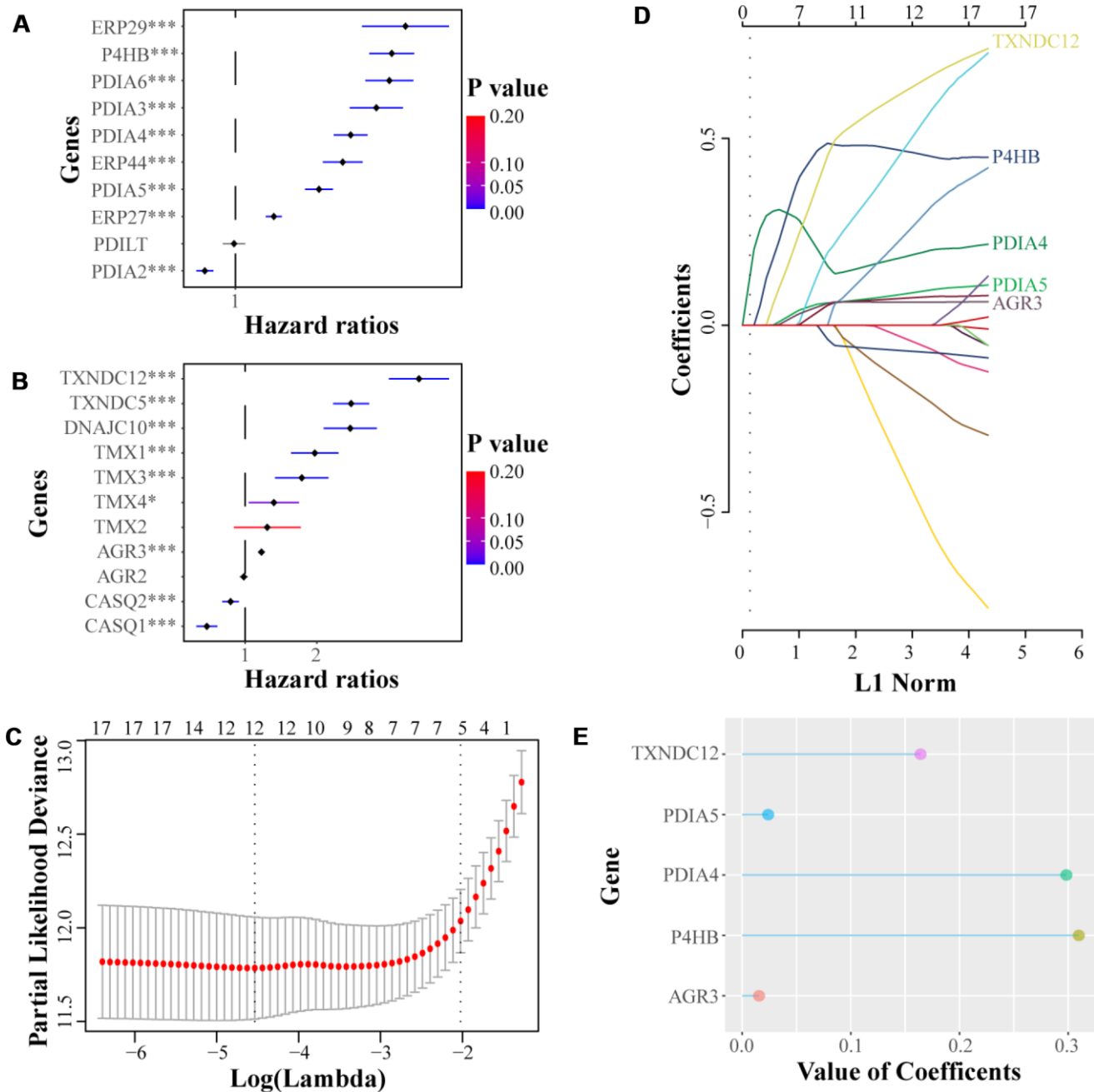

Figure 5. (**A**, **B**) Univariate Cox regression analyses were performed to select significant genes from PDI family according to the clinical information from TCGA. (**C–E**) LASSO coefficients of the significant members of PDI family for OS were calculated, of which the five most influential ones are presented in the figure. * $p < 0.05$, *** $p < 0.001$.

Similarly, the high-risk score was correlated with poor OS in the CGGA datasets (Supplementary Figure 4J–4L). In summary, these findings imply that the PDIs-based model plays an important role in the prediction of patients' clinicopathological characters and prognosis.

Somatic mutations were observed in 149 (94.9%) and 139 (88.54%) of 157 samples in the groups with a low and high-risk score respectively. There were some genes shown mutations in the two groups (low vs. high-risk score): IDH1, TP53, ATRX, TTN, PIK3CA, and
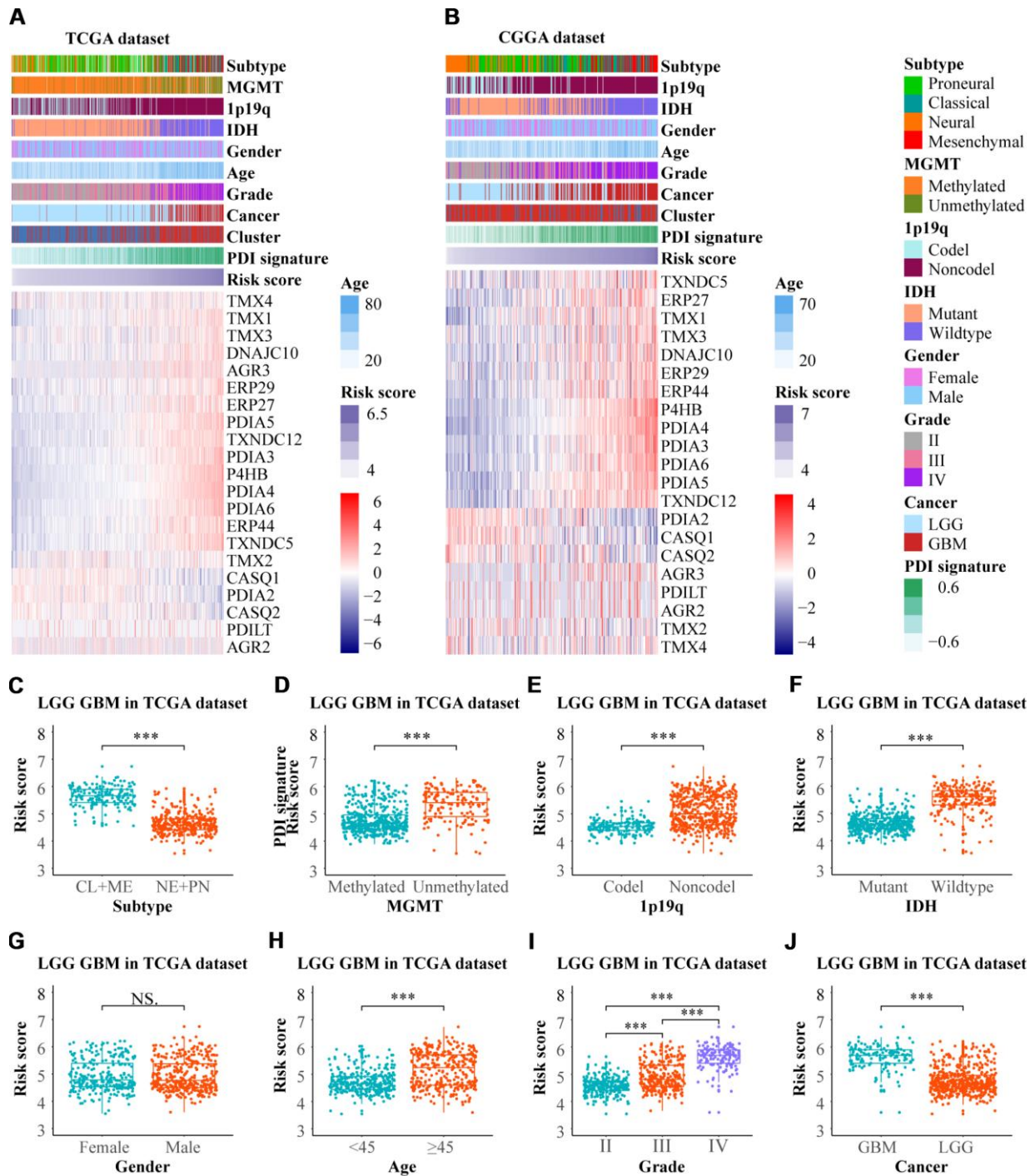

Figure 6. (**A**, **B**) The risk score model of PDI family in gliomas was established on the basis of LASSO coefficients. The distributions of clinical features and PDIs expression according to the risk scores from low to high in TCGA and CGGA are displayed by heat maps. (**C–J**) The risk scores differences between subgroups classified by subtype, MGMT promoter status, 1p19q codel status, IDH status, gender, age, grade, and cancer in LGGGBM cohort. TCGA database as training set and CGGA database as the validation set. *** $p < 0.001$, NS. $p > 0.05$.

MUC16. The frequency of IDH1, TP53, and ATRX mutations was significantly higher in gliomas with low risk score than those with high risk score (IDH1, 87% vs. 8%; TP53, 38% vs. 30%; ATRX, 24% vs. 10%), while the mutation frequency of TTN, PIK3CA, and MUC16 was significantly lower (TTN, 8% vs. 24%; PIK3CA, 6% vs. 11%; MUC16, 3% vs. 15%). Mutations of CIC (28%), FUBP1 (16%), and NOTCH1(12%) in low risk score group and, EGFR (30%), PTEN (25%), NF1 (13%), RYR2 (12%), and RB1 (11%) in high risk score group were identified (Figure 7A, 7B).

SCNAs between samples with low and high-risk scores was investigated considering the somatic copy number alternations' roles in oncogenesis. The incidence of the amplification of Chr 7 together with a deletion of Chr 10 increased with an increase in the value of risk score in gliomas, while the codeletion of 1p/19q decreased (Figure 7C). GISTIC 2.0 analysis identified several significant regions of amplification harboring multiple oncogenes in gliomas with a high-risk score, including 1q32.1 (PIK3C2B), 4q12 (PDGFRA), 7p11·2 (EGFR), and 12q14·1(CDK4). Focal deletion peaks were detected in the group with a high-risk score, such as 9p21·2 (TUSC1), 9p21·3 (CDKN2A, CDKN2B), 10q23·31 (PTEN, FAS), and 10q26·3 (BNIP3). Although the focal amplification and deletion peaks were also present in the low risk score cases, their G values were significantly lower (Figure 7D–7E). Additionally, there were significant genomic regions of amplification (8q23·3, 8q24·21, 11q23·3, 19q13·3) and deletion (1p12, 4q35·2, 14q24·3, 18q23, 19q13·43) observed only in gliomas with low-risk scores (Figure 7E).

The GSVA analysis identified the biological functions of the PDI gene family in gliomas. From the GO and KEGG enrichment analysis, 10 signaling pathways having statistical significance and high correlation coefficient were selected. The higher gene set enrichment scores of all the selected pathways were associated with higher risk scores, excepting for neuron cell-cell adhesion. Some pathways were related to immune response, including T cell apoptotic process, antigen processing and presentation of peptide antigen via MHC class I, regulation of T cell-mediated cytotoxicity, negative regulation of immune response, cytokine-cytokine receptor interaction, and antigen processing and presentation. The cell adhesion-related pathways were also enriched, including neuron cell-cell adhesion, cell adhesion mediated by integrin, cell adhesion molecules CAMs, and focal adhesion. Biological processes significantly associated with the mechanisms of PDIs in gliomas included protein folding in endoplasmic reticulum, regulation of intrinsic apoptotic signaling pathway in response to DNA damage by P53 class mediator, tumor necrosis factor-mediated signaling pathway, regulation of tyrosine phosphorylation of STAT3 protein, ECM receptor interaction, JAK-STAT signaling pathway, amino sugar and nucleotide sugar metabolism, P53 signaling pathway, DNA replication, and mismatch repair (Figure 8A).

Comparisons among PDI signature, cluster, risk score and grade in predicting prognosis and clinical features

ROC analysis compared the PDI signature, risk score, cluster and grade in predicting prognosis and clinical characters. The risk score was the best indicator in predicting 3-year survival, subtype (CL+ME/NE+PN), MGMT status, 1p19q codel status and IDH status. Consensus clustering analysis model was the least performer in predicting prognosis and clinical features (Figure 8B–8F). The Sankey diagrams indicated that glioma patients with high-risk scores had higher PDI signature, higher grade and mainly enriched in cluster1, while the low-risk score was associated with low PDI signature, lower grade and cluster2 (Figure 8G–8H). Besides, there was a positive correlation between risk score and PDI signature (r = 0·84, p < 0.001) (Supplementary Figure 5A).

Constructing prognostic nomogram for overall survival

Univariate and multivariate Cox regression analyses using clinical data downloaded from the TCGA and CGGA database investigated the independent prognostic indicators related to patients' clinical outcomes (OS, DSS, PFI). Risk score (TCGA p = 0·0198, HR = 1·66; CGGA p = 0·0072, HR = 1·56) and 1p19q (TCGA p = 0·0392, HR = 1·84; CGGA p = 2·35E-05, HR = 3·27) were independent prognostic indicators for OS time. Considering parameters of grade III and grade IV with statistical significance, the grade was adopted as one of the prognostic indicators as well (Supplementary Table 1). As shown in Figure 9A–9D, the P value of the global Schoenfeld test and variables were all greater than 0.05, indicating that the model and each variable were satisfied with the PH (proportional hazards) test (global Schoenfeld test p = 0.06675, risk score, p = 0·0632; Grade III, p = 0·1577; Grade IV, p = 0·6294; 1p19q, p = 0·8261). There was no statistical significance in IDH and age in the multivariate Cox regression analysis in CGGA datasets (IDH, p = 0·1604; age, p = 0·5103). Through Cox regression analyses, risk score, WHO grade, IDH, 1p19q, and age were identified as independent factors in predicting DSS, while risk score and IDH were identified as significant prognostic factors of PFI (Supplementary Table 1).

Cox regression model identified three significant prognostic variables which were used to construct the nomogram. Each of the variables was initially assigned a score by finding its position on the corresponding axis. The points of all the variables were added up and the probabilities of the outcomes determined by the location of the total score on the survival axes (Figure 9E). Calibration curves validated the accuracy of the nomogram in TCGA and CGGA and the nomogram-predicted OS corresponded closely with the observed
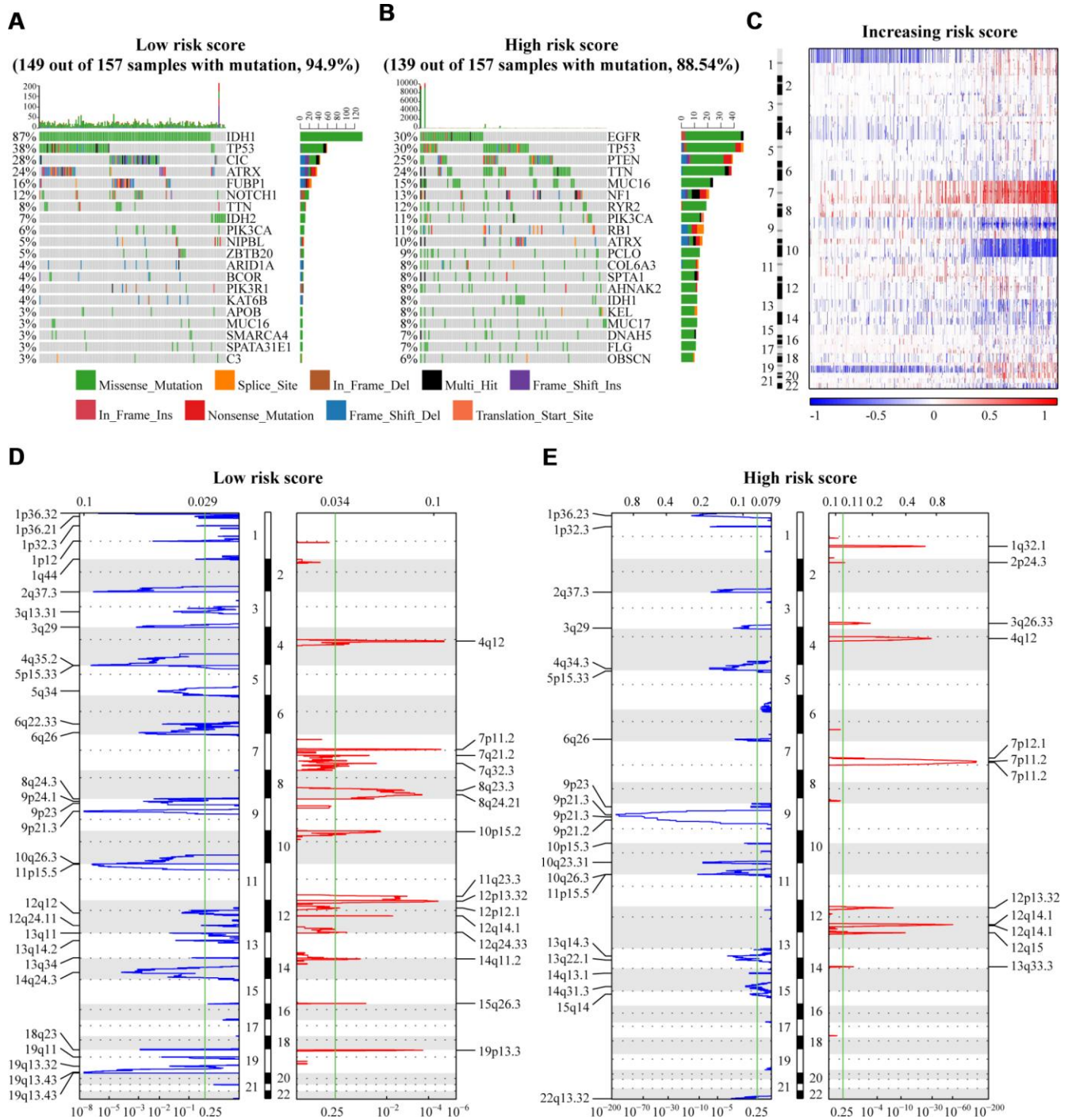

Figure 7. (**A**, **B**) The significantly mutated genes in gliomas were assigned to low and high risk score groups. Here only the top 20 genes with the highest mutation frequency are displayed in figures. (**C**) The overall CNAs profile in order of increasing risk score. (**D**–**E**) GISTIC 2.0 analysis of cases with low and high risk scores revealed chromosomal regions that were significantly deleted (blue) and amplified (red). The green line represents the significance threshold (*q* value=0·25). TCGA database as training set and CGGA database as the validation set.

OS at 3- and 5-year OS (Figure 9F–9G). This data prepared the ROC curve and the AUC values were 0·918 and 0·875 in predicting 3-year and 5-year OS for glioma patients in TCGA, respectively (Figure 9H). A similar process was performed in CGGA, and gave an AUC of 0·862 and 0·875 for the 3- and 5-year OS, respectively (Figure 9I).

The prognostic model value was calculated according to the formula, value $= \beta_1 X_1 + \beta_2 X_2 + \ldots + \beta_n X_n$ (β, regression coefficient; X, prognostic factors). There was a significant difference in the OS between the two groups ($p < 0.0001$) (Supplementary Figure 5B). Similar results were observed in CGGA ($p < 0.0001$) (Supplementary Figure 5C).
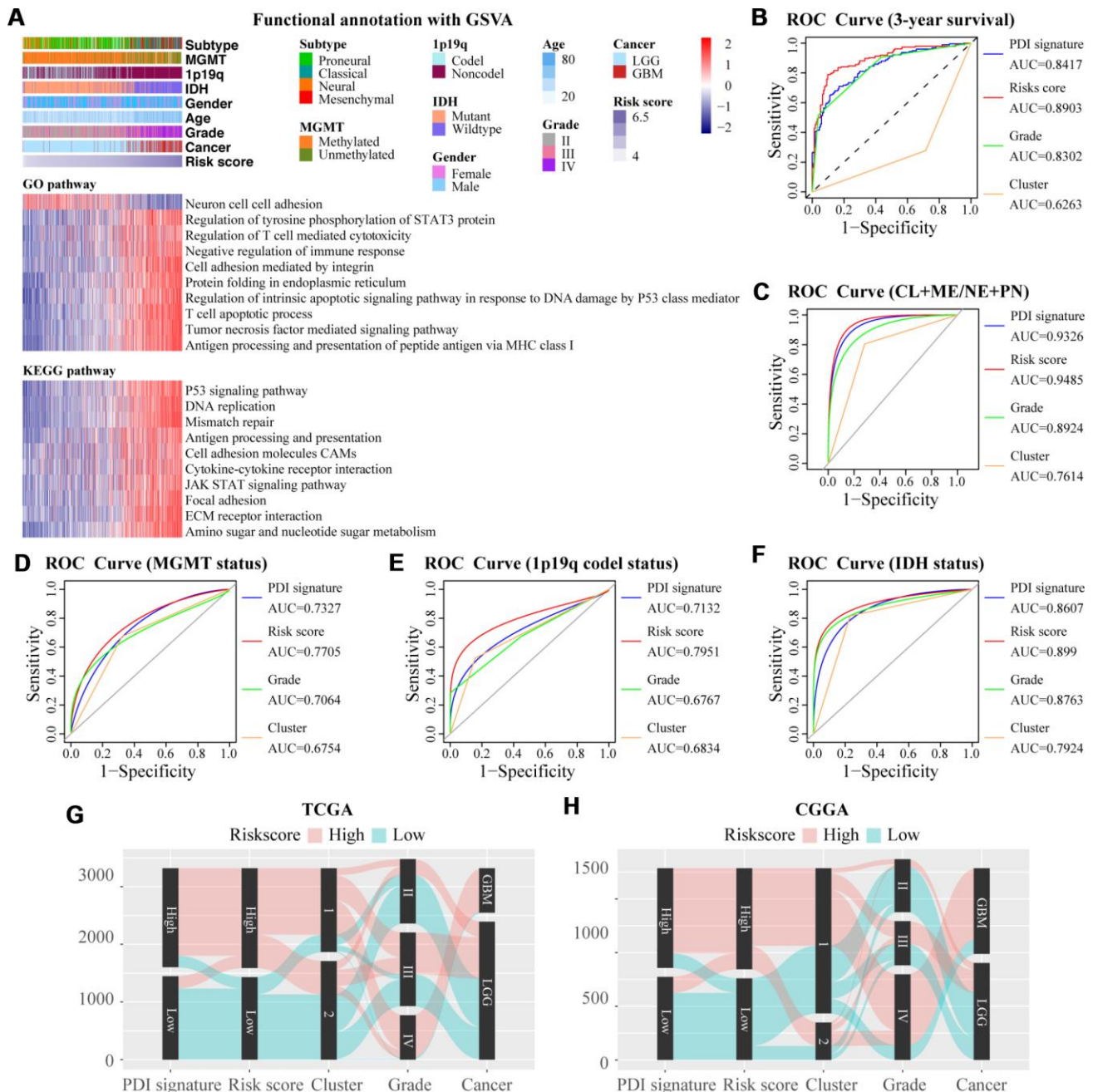

Figure 8. (**A**) GO and KEGG analyses for the PDI gene family and the risk scores determined using GSVA. The heat map shows the distribution of risk scores and clinical features (upper one panel), and gene set enrichment of different pathways (lower two panels). Comparisons of the performance of PDI signature, risk score, grade and cluster in predicting the 3-year overall survival of glioma patients (**B**) subtype (**C**) MGMT promoter status (**D**) 1p19q codel status (**E**) and IDH status (**F**). (**G**, **H**) The relationship among the five indicators, PDI signature, risk score, cluster, WHO grade, and cancer type. TCGA database as training set and CGGA database as the validation set.
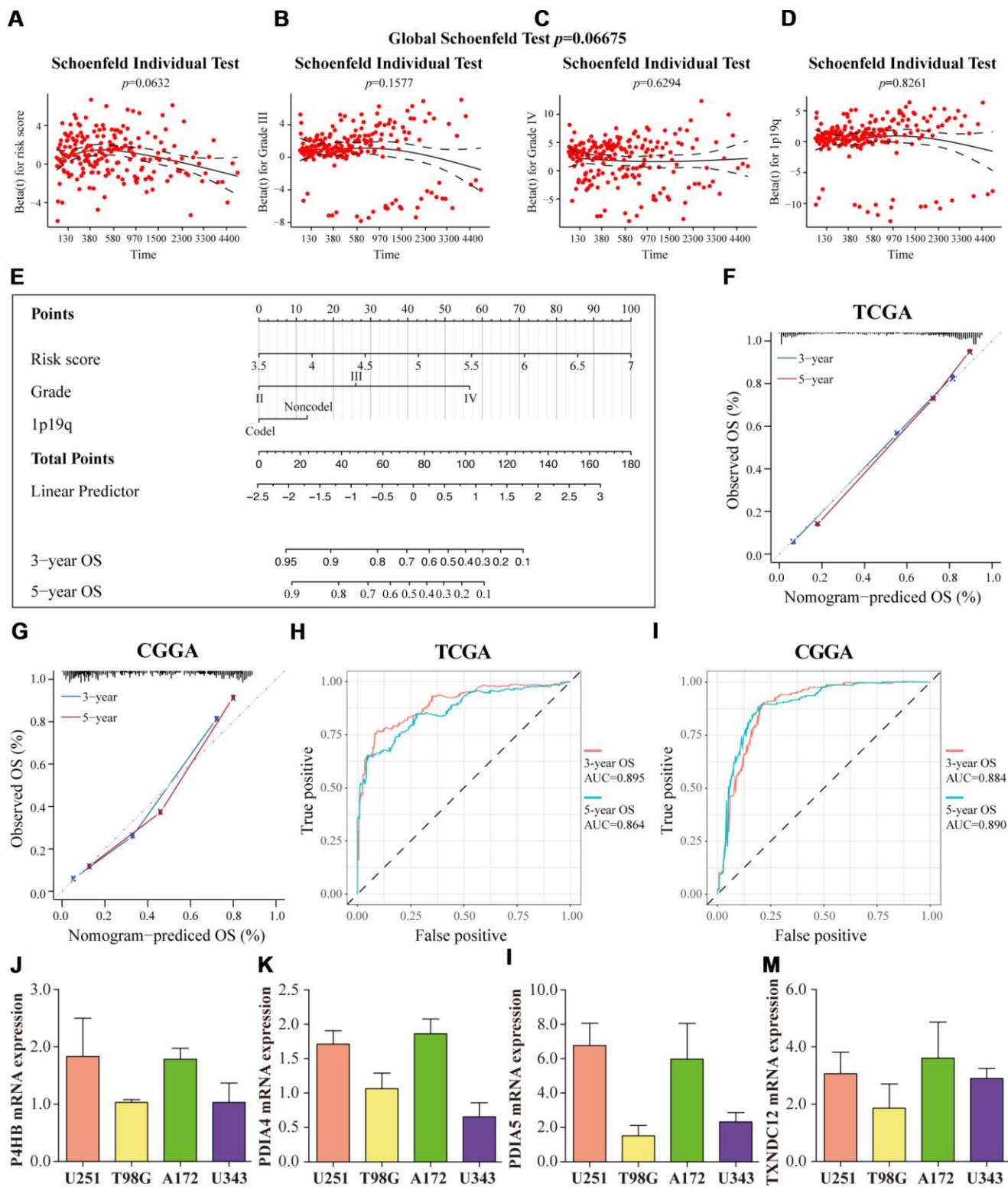
Figure 9. Prognostic nomogram for predicting the 3-year and 5-year overall survival of glioma patients. The Schoenfeld residual plots were displayed for risk score (**A**) Grade III (**B**) Grade IV (**C**) 1p19q (**D**) in the prognostic nomogram. The solid line was a smoothing-spline fit to the plot, with the dashed lines representing the 95% confidence interval. (**E**) Prognostic nomogram for glioma patients was created based on four key characteristics. (**F**, **G**) The calibration curve of OS at 3 years (blue) and 5 years (red). The predicted probability of OS is plotted on the x-axis and the observed OS is plotted on the y-axis. (**H**, **I**) ROC curves from the nomogram of 3-year and 5-year OS. The mRNA expression patterns of P4HB (**J**) PDIA4 (**K**) PDIA5 (**L**) and TXNDC12 (**M**) in glioma cell lines (U251, T98G, A172, U343). TCGA database as training set and CGGA database as the validation set.

The mRNA and protein expression patterns of PDIs in glioma

The qRT-PCR assay was performed to identify significant genes for construction of the risk score model in gliomas. AGR3 was eliminated as it played a non-significant role in this model. As shown in Figure 9J–9M, all four genes, P4HB, PDIA4, PDIA5, and TXNDC12, were expressed in glioma cell lines, and these genes were differentially expressed in different cell lines (U251, T98G, A172, U343).

Furthermore, the immunohistochemistry-based expression data of PDI gene family members was obtained from the online Human Protein Atlas. As shown in Supplementary Figure 5D–5E, the protein expression of P4HB and PDIA4 were higher in glioma tissues compared to normal brain tissues. Additionally, PDIA5 protein was not detected in normal tissues, and it was lowly expressed in cancer tissues (Supplementary Figure 5F). However, the protein expression pattern of TXNDC12 was not presented here due to lack of immunohistochemistry images.

DISCUSSION

In the last three decades, the incidence rate of primary malignant brain and other CNS tumor has increased year by year, with an annual rate of 1%-2%, especially in the elderly population [1]. The average annual age-adjusted incidence rate (AAAIR) of GBM was the highest among malignant brain and other CNS tumors (3.22 per 100,000 population) [2]. Recently, CBTRUS also reported that the median age at diagnosis for GBM was 65 years and survival time was markedly reduced in the elderly patients [2]. Therefore, it is necessary to explore the pathogenesis of glioblastoma to save the older patients from this difficult situation. Dorota et al. showed that PDIA6 was over-expressed in migrating glioma cells and invasive glioma cells, indicating the important role PDIA6 plays in glioma invasion [19]. However, Tae-Wan Kim et al. reported that the inhibition of PDIA6 transduced EGFR signaling via activating and inducing ADAM17 enhanced U87MG cell migration and invasion [20]. However, no study the analyzes the their effects of the twenty-one PDI members on the progression and clinical outcome of gliomas. Therefore, in this study, bioinformatics analysis, GSVA, consensus clustering analysis, and LASSO Cox regression analysis, were used to construct PDI signature, cluster and risk score models of glioma, respectively. The efficacy of PDI signature, risk score and cluster in predicting the clinical characteristics and clinical outcomes were analyzed and compared and risk score was the best indicator. Somatic alterations analysis revealed that gliomas with high PDI signature and risk score were associated with genomic aberrations of driver oncogenes (TTN, MUC16, PIK3CA), but had less mutations of IDH1, TP53, and ATRX. Furthermore, amplification peaks of oncogenes (PIK3C2B, PDGFRA, EGFR, CDK4), and deletion peaks of tumor suppressor genes (TUSC1, CDKN2A, CDKN2B, PTEN, FAS, BNIP3) were detected in the gliomas with a high risk score. These findings revealed that the PDI family are involved in the malignant biological process in gliomas.

GSVA analysis investigated the mechanism of PDIs in gliomas. Consistent with previous studies, the common biological functions of PDIs identified in tumorigenesis and development, included unfolded protein response, endoplasmic reticulum-associated degradation, endoplasmic reticulum stress, cell adhesion, apoptosis, WNT signaling pathways, and cytosolic DNA sensing. There is sufficient evidence supporting that PDI family members are considered as potential targets for tumors due to their functions in UPR, ERAD and ERS signaling pathways. Integrins have been confirmed to be associated with glioma cell invasion, migration and temozolomide resistance [21–23]. Thiol-disulfide exchange reactions in integrins, which play a pivotal role in their activation, are regulated by PDI [15, 19, 23]. Previous studies have not only revealed that PDI is located in the endoplasmic reticulum, which restrains ER stress induction by preventing the accumulation of misfolded proteins which inhibits apoptosis but also suggested that cytosolic PDI is a substrate for caspase-3 and -7 which possesses the anti-apoptotic function [12, 24–27]. Further, Kuo et al. demonstrated that PDIA4 inhibited cell death via preventing the activation/degradation of procaspases-3 and -7 to promote tumor growth and metastasis in lung carcinoma [28].

The findings of function annotation revealed a number of unreported signaling pathways in gliomas which PDIs may be involved in and included P53 signaling pathway, cell cycle, tumor necrosis factor (TNF) mediated signaling pathway, regulation of MAPK cascade, JAK-STAT signaling pathway, positive regulation of NF kappa B transcription factor activity, regulation of tyrosine phosphorylation of STAT3 protein, vascular endothelial growth factor receptor signaling pathway, DNA replication, and mismatch repair. Green et al. noted that PDIA3 was able to interact with P53 to inhibit P53-meditated apoptosis [29]. Similarly, there are studies supporting that PDIs contribute to the regulation of the activity of signaling pathways involved in cellular proliferation, apoptosis, and oncogenesis through interaction with targets, such as TNF, STAT3, NF kappa B [30–33].

An important finding was that PDIs were associated with immune regulation in gliomas, such as negative regulation of immune response, antigen processing and presentation of peptide antigen via MHC class I, T cell receptor signaling pathway, T cell apoptotic process, regulation of T cell-mediated cytotoxicity, antigen processing and presentation, chemokine signaling pathway, B cell receptor signaling pathway, and natural killer cell-mediated cytotoxicity. Gastric cancer patients having high expression of PDIA3 had a favorable prognosis and this was associated with the involvement of PDIA3 in antigen processing and formation of a complex with MCH class I which induced an immune response [34]. However, up-regulation of PDIA3 was associated with poor prognosis in gliomas [17]. Previous studies have shown that the major histocompatibility complex class I chain-related protein A (MICA) is shed from tumor cells via PDIA6 reducing the disulfide bond between them, facilitating the escape of tumor cells from immune responses [18, 35]. These findings demonstrated that the immune response could be explored further to understand the pathogenesis of the PDI family in gliomas.

Considering the important roles of PDI family members in cancer progression, some studies have designed PDIs' inhibitors. Herein, we have briefly reviewed the previously reported inhibitors for PDI family members. Bacitracin, interacting with reduced PDI and then interfering the integrin, inhibits the glioma cell migration and facilitates apoptosis induced by chemotherapy agents in melanoma cells. BAP2 and analogs play key roles in inducing ER stress, decreasing DNA repair proteins' expression, inhibiting cell migration and growth in GBM via binding to His256 in the b domain of PDI [36]. The compounds, as the inhibitor of P4HB and PDIA2, reduce the expression of DNA damage and repair genes [37]. 35GB, the cytotoxic inhibitor of PDI, makes significant contributions in nuclear factor erythroid-2-related factor 2 (Nrf2) antioxidant pathway, ERS response, and autophagy [38]. Previous studies demonstrated that anacardic acid and ribostamycin are able to enhance the cytotoxic activity of TMZ by inhibiting the reductase and chaperone activities of PDIA6 respectively [39]. Besides, there are other compounds functioning as inhibitors of PDIs in cancers, such as T8, ML359, PACMA31, CCF642 [40–43].

In summary, this study the expression patterns, prognostic value, and potential mechanisms of the PDI gene family in gliomas were analyzed. This study was the first to construct clinical models in predicting prognosis and clinicopathological characteristics of glioma and revealed potential signaling pathways. However, further research should be shed light on the validation of PDIs biological impacts on gliomas.

MATERIALS AND METHODS

Datasets analysis

RNA-seq data and corresponding clinical information were downloaded from the TCGA database (http://cancergenome.nih.gov) as training set and from CGGA database (http://www.cgga.org.cn) as the validation set, which was summarized in Supplementary Table 2. Heat maps were then created to visualize differences in PDIs expression.

Gene set variation analysis (GSVA)

The PDI signature for each glioma sample was established using GSVA, a non-parametric and unsupervised algorithm. The heat maps and box plots were used to illustrate the relationship between PDI signature and PDIs mRNA expressions and clinical features of gliomas. The functional enrichment analysis was performed using "GSVA package" to reveal the potential signaling pathways of PDIs involved in glioma, setting |correlation coefficient| > 0·5 as the cutoff value [44]. Gene Ontology (GO) terms and Kyoto Encyclopedia of Genes and Genomes (KEGG) pathways were obtained from Molecular Signatures Database (MSigDB) [45].

Consensus clustering analysis

To create clusters of gliomas based on members with similar intrinsic features of PDIs mRNA expression, samples were grouped into distinct subgroups by consensus clustering analysis with the R package "ConsensusClusterPlus" [46]. The subsampling parameter was 80% with 1000 times and k (the number of clusters) ranged from 2 to 10. The optimal number of clusters was determined according to cumulative distribution function plots and consensus matrices [47]. Differences in PDIs expression and clinical features of glioma between clusters were visualized by heat maps.

Least absolute shrinkage and selection operator (LASSO) Cox regression

The LASSO Cox regression was used to construct a PDIs-based survival risk assessment model. Prognostic PDI family members were used to calculate the LASSO coefficients, according to the highest lambda value through Lasso method (lambda 1se) with 10-fold cross validation [48]. Subsequently, the risk score model of glioma was established based on LASSO coefficients. The association between risk score and PDIs expression and clinical characters was illustrated by heat maps and box plots.

Survival analysis

Glioma patients were divided into high and low groups on the basis of median PDI signature or risk score. Survival curves were created by the Kaplan-Meier method with log-rank test, comparing the overall survival (OS), progression free interval (PFI), and disease specific survival (DSS) rates of patients in low and high group. Additionally, survival analyses were conducted between clusters of gliomas.

Analysis of genetic alterations in gliomas

We further investigated genetic alterations in gliomas, including somatic mutations and somatic copy number alternations (SCNAs), based on samples obtained from TCGA database. Glioma samples were divided into four groups according to the values of PDI signature and risk scores of low and high groups. Thereafter, the top 20 genes with the highest mutation frequency in the 1st (lowest) and 4th (highest) groups were screened and presented. In addition, Genomic Identification of Significant Targets in Cancer 2·0 (GISTIC) was used to explore SCNAs between the two groups classified by median value of risk score, according to the gene copy number variation data and Human genome reference consortium h19 downloaded from TCGA and GISTIC 2·0 [49]. The threshold copy number at alteration peaks were derived from GISTIC analysis.

Receiver operating characteristic (ROC)

ROC and the area under the curve (AUC) were used to compare the prediction performance of PDI signature, risk score, clustering and grade in several aspects, including 3-year OS, subtype (CL+ME, NE+PN), MGMT status (methylated, unmethylated), 1p19q codel status (codel, noncodel), and IDH status (wildtype, mutant).

Cox regression analysis and nomogram construction

The univariate and multivariate Cox regression analyses were performed to identify prognostic factors with P value < 0·05 for designing a prognostic model. A nomogram was constructed using the "RMS" [50, 51] in R software to predict 3- and 5-year OS in accordance with the results of multivariate Cox regression analyses. The prediction accuracy of the nomogram for OS was evaluated by a calibration curve and AUC. Furthermore, the accuracy of the prognostic models was also validated in CGGA dataset.

Cell culture

Human glioma cell lines (U251, T98G, A172, U343) were obtained from the Chinese Academy of Sciences (Shanghai, China). All cells were maintained in Dulbecco's modified Eagle's medium (DMEM) (Gibco, CA, USA) supplemented with 10% fetal bovine serum (FBS) (Gibco, CA, USA) at 37°C with 5% CO_2.

Quantitative real-time polymerase chain reaction (qRT-PCR) analysis

Total RNA was extracted from cells using RNAiso Plus reagent (Gibco, CA, USA) according to manufacturer's instructions. The total RNA was reverse-transcribed into cDNA using the PrimeScript RT Master Mix (Takara, China) kit following the manufacturer's recommendations. The qRT-PCR was conducted with the SYBR® Premix DimerEraserTM (Takara, China) on the LightCycler® 480 system (Roche Diagnostics, Basel, Switzerland). The following primer sequences were used: P4HB forward primer, 5′-GGTGCTGCGGAAAAGCAA C-3′ and reverse primer, 5′-ACCTGATCTCGGAACCT TCTG-3′; PDIA4 forward primer, 5′-GGCAGGCTGT AGACTACGAG-3′ and reverse primer, 5′-TTGGTCAA CACAAGCGTGACT-3′; PDIA5 forward primer, 5′-AAAGGTCTCCTCGCTCATTGA-3′ and reverse primer, 5′-CACCAGTACATTATTCCGGGTTC-3′; TXNDC12 forward primer, 5′-TGGCAAGGTGCATCCTGAAAT-3′ and reverse primer, 5′-TGCTCGGCACTGACATAA AAA-3′. GAPDH was used as the internal reference gene for data normalization. The qRT-PCR reaction steps were as follows: denaturation at 95°C for 30 sec, followed by 45 cycles of 95°C for 5 sec and 60°C for 20 sec. The relative mRNA expression was analyzed using the $2^{-\Delta\Delta Ct}$ method.

The human protein atlas and 3D protein structure

The immunohistochemical assay images of different PDI family members in the normal and high grade glioma tissues were downloaded from the Human Protein Atlas website (https://www.proteinatlas.org) [52, 53].

Statistical analysis

All statistical analyses were conducted using R software (version 3·5·3). Differences between groups were assessed using the two-tailed Students' t-test. Multiple groups were compared by one-way ANOVA test. The Schoenfeld residual plots was performed to assess the PH assumption. Univariate and multivariate Cox regression analyses were performed to determine the prognostic value of the risk score and clinical features. The partition around medoids (PAM) algorithm has been conducted in the consensus clustering analysis. The chi-squared test was performed, while analyzing clinical characteristics' difference between cluster 1 and 2. Kaplan-Meier method with log-rank

test was used to compare the OS, PFI and DSS rates of glioma patients (low-/high-PDI signature, low-/high-risk score, cluster 1/2). The correlation between two variables was analyzed with Spearman rank. $p < 0\cdot05$ was considered to indicate statistical significance.

AUTHOR CONTRIBUTIONS

QC, ZxL, ZgP, and YC conceived and designed the idea for the manuscript and wrote the paper. XW, HcZ, WjZ, ZwX, JqH, and HC contributed the collection, analysis, and interpretation of data. NZ provided analysis tools. All authors gave approval for this version of the manuscript to be published, and agree to be accountable for all aspects of the work.

CONFLICTS OF INTEREST

The authors declare that there are no potential conflicts of interest.

REFERENCES

1. Ostrom QT, Gittleman H, Farah P, Ondracek A, Chen Y, Wolinsky Y, Stroup NE, Kruchko C, Barnholtz-Sloan JS. CBTRUS statistical report: primary brain and central nervous system tumors diagnosed in the United States in 2006-2010. Neuro Oncol. 2013 (Suppl 2); 15:ii1–56.
https://doi.org/10.1093/neuonc/not151
PMID:24137015

2. Ostrom QT, Cioffi G, Gittleman H, Patil N, Waite K, Kruchko C, Barnholtz-Sloan JS. CBTRUS Statistical Report: Primary Brain and Other Central Nervous System Tumors Diagnosed in the United States in 2012-2016. Neuro Oncol. 2019; 21:v1–v100.
https://doi.org/10.1093/neuonc/noz150
PMID:31675094

3. Nakamura H, Makino K, Yano S, Kuratsu J, and Kumamoto Brain Tumor Research Group. Epidemiological study of primary intracranial tumors: a regional survey in Kumamoto prefecture in southern Japan—20-year study. Int J Clin Oncol. 2011; 16:314–21.
https://doi.org/10.1007/s10147-010-0178-y
PMID:21240684

4. Verhaak RG, Hoadley KA, Purdom E, Wang V, Qi Y, Wilkerson MD, Miller CR, Ding L, Golub T, Mesirov JP, Alexe G, Lawrence M, O'Kelly M, et al, and Cancer Genome Atlas Research Network. Integrated genomic analysis identifies clinically relevant subtypes of glioblastoma characterized by abnormalities in PDGFRA, IDH1, EGFR, and NF1. Cancer Cell. 2010; 17:98–110.
https://doi.org/10.1016/j.ccr.2009.12.020
PMID:20129251

5. Wanggou S, Feng C, Xie Y, Ye L, Wang F, Li X. Sample Level Enrichment Analysis of KEGG Pathways Identifies Clinically Relevant Subtypes of Glioblastoma. J Cancer. 2016; 7:1701–10.
https://doi.org/10.7150/jca.15486 PMID:27698907

6. Zhang H, Wang R, Yu Y, Liu J, Luo T, Fan F. Glioblastoma Treatment Modalities besides Surgery. J Cancer. 2019; 10:4793–4806.
https://doi.org/10.7150/jca.32475
PMID:31598150

7. Long W, Yi Y, Chen S, Cao Q, Zhao W, Liu Q. Potential New Therapies for Pediatric Diffuse Intrinsic Pontine Glioma. Front Pharmacol. 2017; 8:495.
https://doi.org/10.3389/fphar.2017.00495
PMID:28790919

8. Wick W, Osswald M, Wick A, Winkler F. Treatment of glioblastoma in adults. Ther Adv Neurol Disord. 2018; 11:1756286418790452.
https://doi.org/10.1177/1756286418790452
PMID:30083233

9. Yi X, Cao H, Tang H, Gong G, Hu Z, Liao W, Sun L, Chen BT, Li X. Gliosarcoma: a clinical and radiological analysis of 48 cases. Eur Radiol. 2019; 29:429–38.
https://doi.org/10.1007/s00330-018-5398-y
PMID:29948068

10. Galligan JJ, Petersen DR. The human protein disulfide isomerase gene family. Hum Genomics. 2012; 6:6.
https://doi.org/10.1186/1479-7364-6-6
PMID:23245351

11. Lee E, Lee DH. Emerging roles of protein disulfide isomerase in cancer. BMB Rep. 2017; 50:401–10.
https://doi.org/10.5483/BMBRep.2017.50.8.107
PMID:28648146

12. Xu S, Sankar S, Neamati N. Protein disulfide isomerase: a promising target for cancer therapy. Drug Discov Today. 2014; 19:222–40. https://doi.org/10.1016/j.drudis.2013.10.017 PMID:24184531

13. Cheng HP, Liu Q, Li Y, Li XD, Zhu CY. The Inhibitory Effect of PDIA6 Downregulation on Bladder Cancer Cell Proliferation and Invasion. Oncol Res. 2017; 25:587–93. https://doi.org/10.3727/096504016X14761811155298 PMID:27760590

14. Samanta S, Tamura S, Dubeau L, Mhawech-Fauceglia P, Miyagi Y, Kato H, Lieberman R, Buckanovich RJ, Lin YG, Neamati N. Expression of protein disulfide isomerase family members correlates with tumor progression and patient survival in ovarian cancer. Oncotarget. 2017; 8:103543–56. https://doi.org/10.18632/oncotarget.21569 PMID:29262583

15. Li S, Li C, Ryu HH, Lim SH, Jang WY, Jung S. Bacitracin Inhibits the Migration of U87-MG Glioma Cells via Interferences of the Integrin Outside-in Signaling Pathway. J Korean Neurosurg Soc. 2016; 59:106–16. https://doi.org/10.3340/jkns.2016.59.2.106 PMID:26962415

16. Sun S, Lee D, Ho AS, Pu JK, Zhang XQ, Lee NP, Day PJ, Lui WM, Fung CF, Leung GK. Inhibition of prolyl 4-hydroxylase, beta polypeptide (P4HB) attenuates temozolomide resistance in malignant glioma via the endoplasmic reticulum stress response (ERSR) pathways. Neuro Oncol. 2013; 15:562–77. https://doi.org/10.1093/neuonc/not005 PMID:23444257

17. Zou H, Wen C, Peng Z, Shao YY, Hu L, Li S, Li C, Zhou HH. P4HB and PDIA3 are associated with tumor progression and therapeutic outcome of diffuse gliomas. Oncol Rep. 2018; 39:501–10. https://doi.org/10.3892/or.2017.6134 PMID:29207176

18. Horibe T, Torisawa A, Masuda Y, Kawakami K. Functional analysis of protein disulfide isomerase P5 in glioblastoma cells as a novel anticancer target. Oncol Rep. 2019; 41:961–72. https://doi.org/10.3892/or.2018.6868 PMID:30431130

19. Goplen D, Wang J, Enger PO, Tysnes BB, Terzis AJ, Laerum OD, Bjerkvig R. Protein disulfide isomerase expression is related to the invasive properties of malignant glioma. Cancer Res. 2006; 66:9895–902. https://doi.org/10.1158/0008-5472.CAN-05-4589 PMID:17047051

20. Kim TW, Ryu HH, Li SY, Li CH, Lim SH, Jang WY, Jung S. PDIA6 regulation of ADAM17 shedding activity and EGFR-mediated migration and invasion of glioblastoma cells. J Neurosurg. 2017; 126:1829–38. https://doi.org/10.3171/2016.5.JNS152831 PMID:27540907

21. Janouskova H, Maglott A, Leger DY, Bossert C, Noulet F, Guerin E, Guenot D, Pinel S, Chastagner P, Plenat F, Entz-Werle N, Lehmann-Che J, Godet J, et al. Integrin α5β1 plays a critical role in resistance to temozolomide by interfering with the p53 pathway in high-grade glioma. Cancer Res. 2012; 72:3463–70. https://doi.org/10.1158/0008-5472.CAN-11-4199 PMID:22593187

22. Ma J, Cui W, He SM, Duan YH, Heng LJ, Wang L, Gao GD. Human U87 astrocytoma cell invasion induced by interaction of βig-h3 with integrin α5β1 involves calpain-2. PLoS One. 2012; 7:e37297. https://doi.org/10.1371/journal.pone.0037297 PMID:22629380

23. Tysnes BB, Mahesparan R. Biological mechanisms of glioma invasion and potential therapeutic targets. J Neurooncol. 2001; 53:129–47. https://doi.org/10.1023/A:1012249216117 PMID:11716066

24. Lovat PE, Corazzari M, Armstrong JL, Martin S, Pagliarini V, Hill D, Brown AM, Piacentini M, Birch-Machin MA, Redfern CP. Increasing melanoma cell death using inhibitors of protein disulfide isomerases to abrogate survival responses to endoplasmic reticulum stress. Cancer Res. 2008; 68:5363–69. https://doi.org/10.1158/0008-5472.CAN-08-0035 PMID:18593938

25. Muller C, Bandemer J, Vindis C, Camaré C, Mucher E, Guéraud F, Larroque-Cardoso P, Bernis C, Auge N, Salvayre R, Negre-Salvayre A. Protein disulfide isomerase modification and inhibition contribute to ER stress and apoptosis induced by oxidized low density lipoproteins. Antioxid Redox Signal. 2013; 18:731–42. https://doi.org/10.1089/ars.2012.4577 PMID:23083489

26. Na KS, Park BC, Jang M, Cho S, Lee DH, Kang S, Lee CK, Bae KH, Park SG. Protein disulfide isomerase is cleaved by caspase-3 and -7 during apoptosis. Mol Cells. 2007; 24:261–67. PMID:17978580

27. Wang M, Ye R, Barron E, Baumeister P, Mao C, Luo S, Fu Y, Luo B, Dubeau L, Hinton DR, Lee AS. Essential role of the unfolded protein response regulator GRP78/BiP in protection from neuronal apoptosis. Cell Death Differ. 2010; 17:488–98. https://doi.org/10.1038/cdd.2009.144 PMID:19816510

28. Kuo TF, Chen TY, Jiang ST, Chen KW, Chiang YM, Hsu YJ, Liu YJ, Chen HM, Yokoyama KK, Tsai KC, Yeh HH, Chen YR, Yang MT, et al. Protein disulfide isomerase a4 acts as a novel regulator of cancer growth through the

procaspase pathway. Oncogene. 2017; 36:5484–96. https://doi.org/10.1038/onc.2017.156 PMID:28534513

29. Green DR, Kroemer G. Cytoplasmic functions of the tumour suppressor p53. Nature. 2009; 458:1127–30. https://doi.org/10.1038/nature07986 PMID:19407794

30. Hettinghouse A, Liu R, Liu CJ. Multifunctional molecule ERp57: from cancer to neurodegenerative diseases. Pharmacol Ther. 2018; 181:34–48. https://doi.org/10.1016/j.pharmthera.2017.07.011 PMID:28723413

31. Wu W, Beilhartz G, Roy Y, Richard CL, Curtin M, Brown L, Cadieux D, Coppolino M, Farach-Carson MC, Nemere I, Meckling KA. Nuclear translocation of the 1,25D3-MARRS (membrane associated rapid response to steroids) receptor protein and NFkappaB in differentiating NB4 leukemia cells. Exp Cell Res. 2010; 316:1101–08. https://doi.org/10.1016/j.yexcr.2010.01.010 PMID:20064506

32. Yang WS, Yu H, Kim JJ, Lee MJ, Park SK. Vitamin D-induced ectodomain shedding of TNF receptor 1 as a nongenomic action: D3 vs D2 derivatives. J Steroid Biochem Mol Biol. 2016; 155:18–25. https://doi.org/10.1016/j.jsbmb.2015.09.019 PMID:26385608

33. Zhu Y, Cai L, Guo J, Chen N, Yi X, Zhao Y, Cai J, Wang Z. Depletion of Dicer promotes epithelial ovarian cancer progression by elevating PDIA3 expression. Tumour Biol. 2016; 37:14009–23. https://doi.org/10.1007/s13277-016-5218-4 PMID:27492604

34. Shimoda T, Wada R, Kure S, Ishino K, Kudo M, Ohashi R, Fujita I, Uchida E, Yoshida H, Naito Z. Expression of protein disulfide isomerase A3 and its clinicopathological association in gastric cancer. Oncol Rep. 2019; 41:2265–72. https://doi.org/10.3892/or.2019.6999 PMID:30720117

35. Kaiser BK, Yim D, Chow IT, Gonzalez S, Dai Z, Mann HH, Strong RK, Groh V, Spies T. Disulphide-isomerase-enabled shedding of tumour-associated NKG2D ligands. Nature. 2007; 447:482–86. https://doi.org/10.1038/nature05768 PMID:17495932

36. Yang S, Shergalis A, Lu D, Kyani A, Liu Z, Ljungman M, Neamati N. Design, Synthesis, and Biological Evaluation of Novel Allosteric Protein Disulfide Isomerase Inhibitors. J Med Chem. 2019; 62:3447–74. https://doi.org/10.1021/acs.jmedchem.8b01951 PMID:30759340

37. Xu S, Liu Y, Yang K, Wang H, Shergalis A, Kyani A, Bankhead A 3rd, Tamura S, Yang S, Wang X, Wang CC, Rehemtulla A, Ljungman M, Neamati N. Inhibition of protein disulfide isomerase in glioblastoma causes marked downregulation of DNA repair and DNA damage response genes. Theranostics. 2019; 9:2282–98. https://doi.org/10.7150/thno.30621 PMID:31149044

38. Kyani A, Tamura S, Yang S, Shergalis A, Samanta S, Kuang Y, Ljungman M, Neamati N. Discovery and Mechanistic Elucidation of a Class of Protein Disulfide Isomerase Inhibitors for the Treatment of Glioblastoma. ChemMedChem. 2018; 13:164–77. https://doi.org/10.1002/cmdc.201700629 PMID:29235250

39. Ko MK, Kay EP. PDI-mediated ER retention and proteasomal degradation of procollagen I in corneal endothelial cells. Exp Cell Res. 2004; 295:25–35. https://doi.org/10.1016/j.yexcr.2003.12.013 PMID:15051487

40. Eirich J, Braig S, Schyschka L, Servatius P, Hoffmann J, Hecht S, Fulda S, Zahler S, Antes I, Kazmaier U, Sieber SA, Vollmar AM. A small molecule inhibits protein disulfide isomerase and triggers the chemosensitization of cancer cells. Angew Chem Int Ed Engl. 2014; 53:12960–65. https://doi.org/10.1002/anie.201406577 PMID:25256790

41. Khodier C, VerPlank L, Nag PP, Pu J, Wurst J, Pilyugina T, Dockendorff C, Galinski CN, Scalise AA, Passam F, van Hessem L, Dilks J, Kennedy DR, et al. Identification of ML359 as a Small Molecule Inhibitor of Protein Disulfide Isomerase. Probe Reports from the NIH Molecular Libraries Program. 2014. Bethesda (MD): National Center for Biotechnology Information (US); 2010-. PMID:24624466

42. Vatolin S, Phillips JG, Jha BK, Govindgari S, Hu J, Grabowski D, Parker Y, Lindner DJ, Zhong F, Distelhorst CW, Smith MR, Cotta C, Xu Y, et al. Novel Protein Disulfide Isomerase Inhibitor with Anticancer Activity in Multiple Myeloma. Cancer Res. 2016; 76:3340–50. https://doi.org/10.1158/0008-5472.CAN-15-3099 PMID:27197150

43. Xu S, Butkevich AN, Yamada R, Zhou Y, Debnath B, Duncan R, Zandi E, Petasis NA, Neamati N. Discovery of an orally active small-molecule irreversible inhibitor of protein disulfide isomerase for ovarian cancer treatment. Proc Natl Acad Sci USA. 2012; 109:16348–53. https://doi.org/10.1073/pnas.1205226109 PMID:22988091

44. Hänzelmann S, Castelo R, Guinney J. GSVA: gene set variation analysis for microarray and RNA-seq data. BMC Bioinformatics. 2013; 14:7. https://doi.org/10.1186/1471-2105-14-7

PMID:23323831

45. Liberzon A, Birger C, Thorvaldsdóttir H, Ghandi M, Mesirov JP, Tamayo P. The Molecular Signatures Database (MSigDB) hallmark gene set collection. Cell Syst. 2015; 1:417–25.
https://doi.org/10.1016/j.cels.2015.12.004
PMID:26771021

46. Wilkerson MD, Hayes DN. ConsensusClusterPlus: a class discovery tool with confidence assessments and item tracking. Bioinformatics. 2010; 26:1572–73.
https://doi.org/10.1093/bioinformatics/btq170
PMID:20427518

47. Datta S, Datta S. Comparisons and validation of statistical clustering techniques for microarray gene expression data. Bioinformatics. 2003; 19:459–66.
https://doi.org/10.1093/bioinformatics/btg025
PMID:12611800

48. Goeman JJ. L1 penalized estimation in the Cox proportional hazards model. Biom J. 2010; 52:70–84.
https://doi.org/10.1002/bimj.200900028
PMID:19937997

49. Mermel CH, Schumacher SE, Hill B, Meyerson ML, Beroukhim R, Getz G. GISTIC2.0 facilitates sensitive and confident localization of the targets of focal somatic copy-number alteration in human cancers. Genome Biol. 2011; 12:R41.

https://doi.org/10.1186/gb-2011-12-4-r41
PMID:21527027

50. Núñez E, Steyerberg EW, Núñez J. [Regression modeling strategies]. Rev Esp Cardiol. 2011; 64:501–07.
https://doi.org/10.1016/j.recesp.2011.01.019
PMID:21531065

51. Nick TG, Hardin JM. Regression modeling strategies: an illustrative case study from medical rehabilitation outcomes research. Am J Occup Ther. 1999; 53:459–70.
https://doi.org/10.5014/ajot.53.5.459 PMID:10500854

52. Uhlén M, Fagerberg L, Hallström BM, Lindskog C, Oksvold P, Mardinoglu A, Sivertsson Å, Kampf C, Sjöstedt E, Asplund A, Olsson I, Edlund K, Lundberg E, et al. Proteomics. Tissue-based map of the human proteome. Science. 2015; 347:1260419.
https://doi.org/10.1126/science.1260419
PMID:25613900

53. Thul PJ, Åkesson L, Wiking M, Mahdessian D, Geladaki A, Ait Blal H, Alm T, Asplund A, Björk L, Breckels LM, Bäckström A, Danielsson F, Fagerberg L, et al. A subcellular map of the human proteome. Science. 2017; 356:eaal3321.
https://doi.org/10.1126/science.aal3321
PMID:28495876
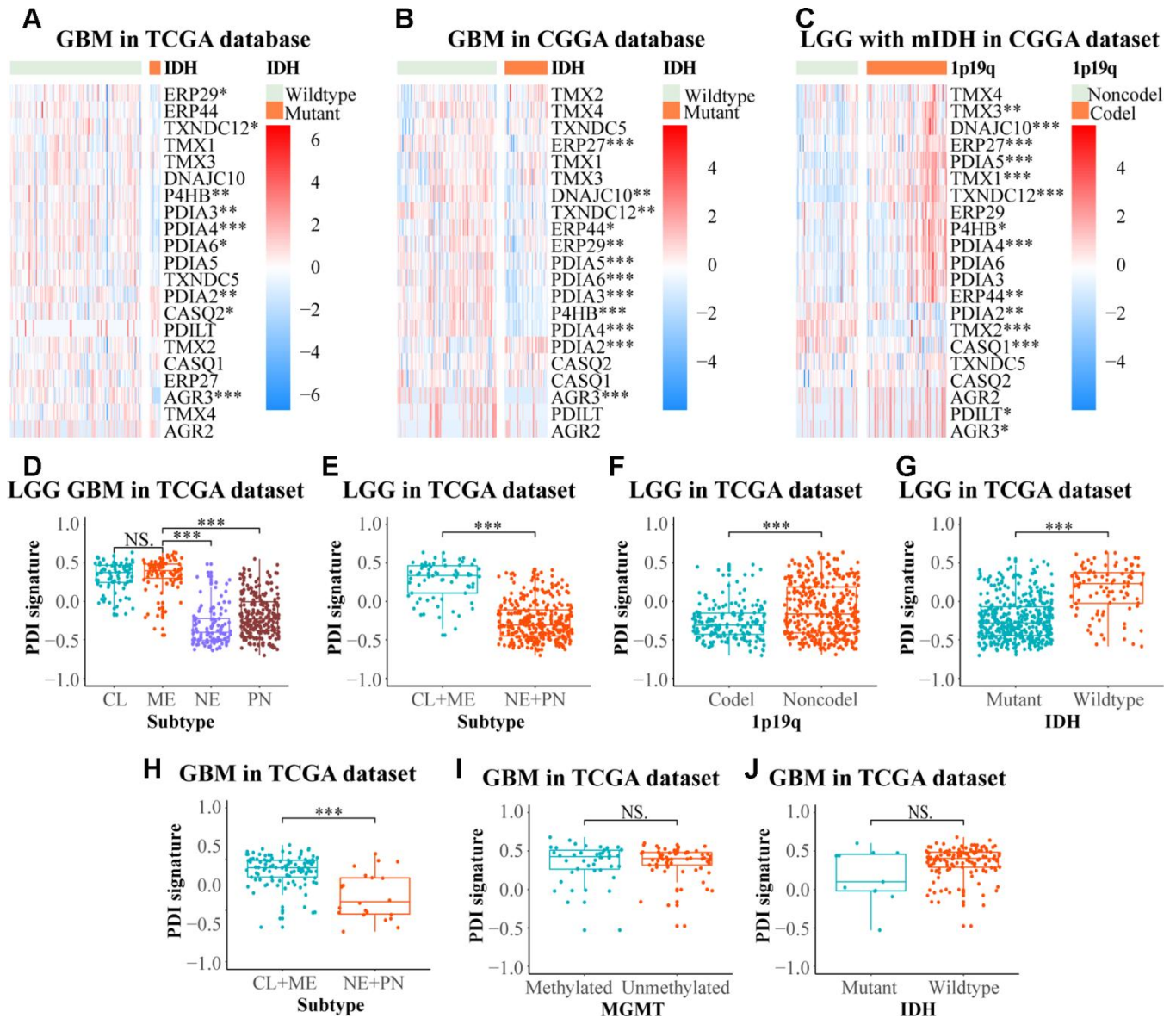
Supplementary Figure 1. (**A**, **B**) The mRNA expression patterns of PDIs in GBM with different status of IDH from TCGA and CGGA datasets. (**C**) The mRNA expression patterns of PDIs in LGG with different status of 1p19q from CGGA dataset. (**D**–**J**) In TCGA dataset, the distribution of PDI signature in gliomas was classified by subtype, 1p19q codel status, IDH status and MGMT promoter status. TCGA database as training set and CGGA database as the validation set. * P<0.05, ** P<0.01, ***P<0.001, NS. P>0.05.
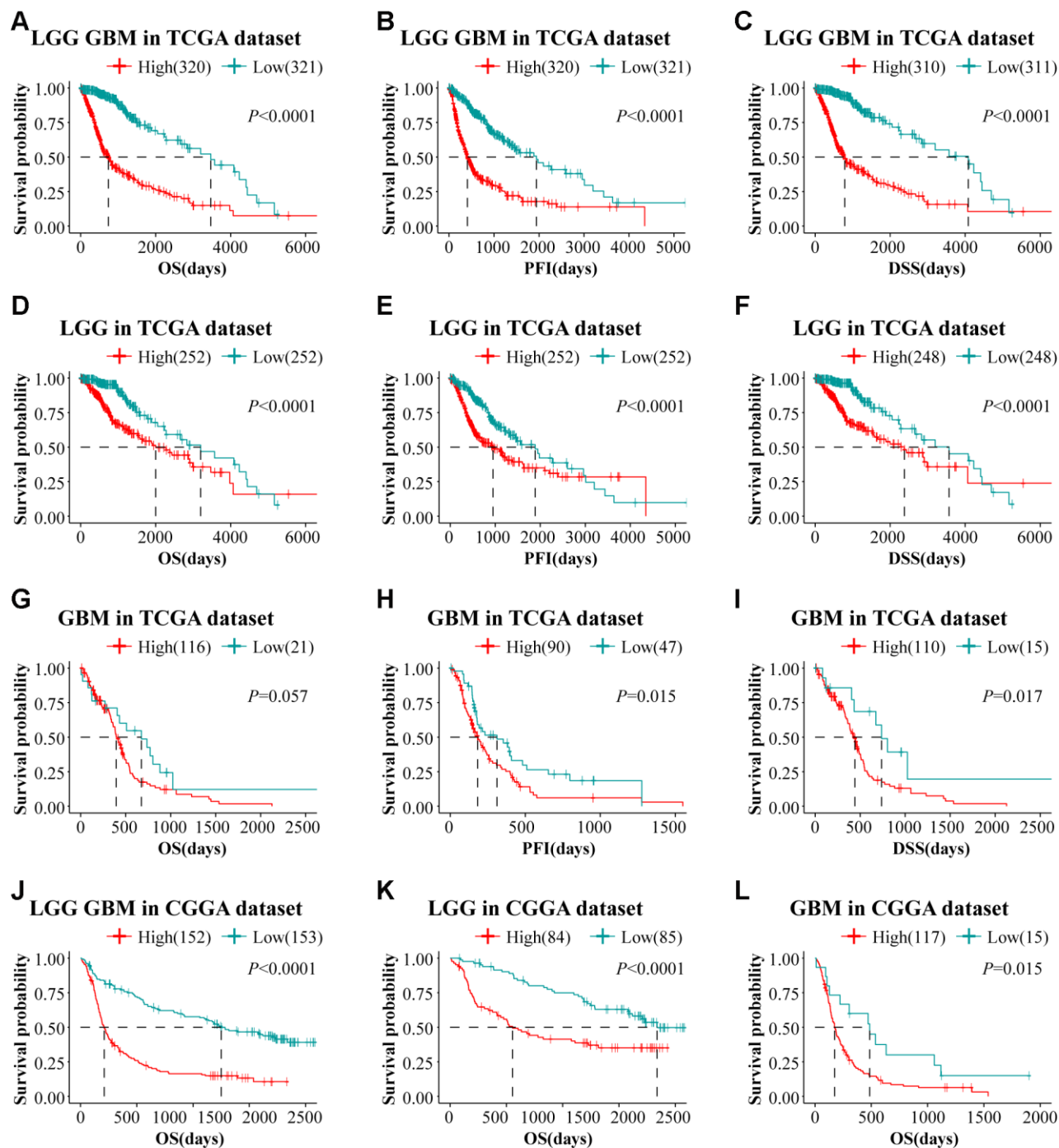
Supplementary Figure 2. The prognostic value of PDI signature in patients with gliomas. Kaplan-Meier survival curves for the OS, PFI and DSS, based on the value of PDI signature in LGGGBM (**A**–**C**), LGG (**D**–**F**), and GBM (**G**–**I**) samples downloaded from TCGA. (**J**–**L**) The survival curves of OS were constructed based on the CCGA datasets. TCGA database as training set and CGGA database as the validation set. CV, cut-off value used to divide patients into high and low groups.
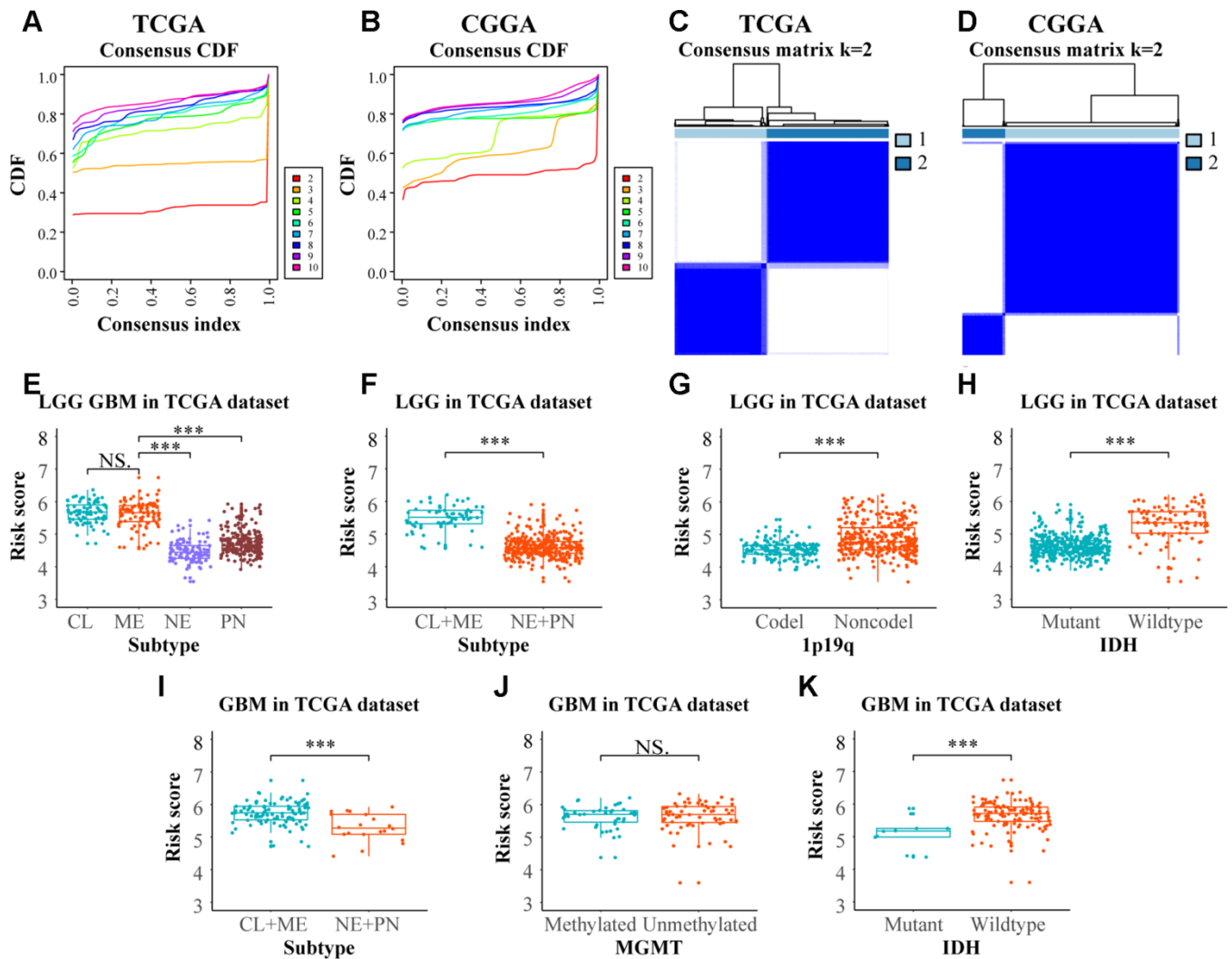
Supplementary Figure 3. (**A**, **B**) Clustering by the consensus clustering algorithm with k= 2 to 10. The cumulative distribution function (CDF) plot of the PDIs mRNA expression in gliomas from TCGA and CGGA. k=2 was defined as the optimal number. (**C**, **D**) Consensus matrix for 2 clusters. The dark blue rectangles show the samples assigned to the 2 clusters while the light blue lines represent the unassigned samples. Comparisons of risk score values between subgroups separated by clinicopathological characters. Differences in risk scores in LGGGBM (e), LGG (**F**, **H**) and GBM (**I**, **K**) classified by subtype, 1p19q codel status, IDH status and MGMT promoter status. ***P<0.001, NS P>0.05. TCGA database as training set and CGGA database as the validation set.
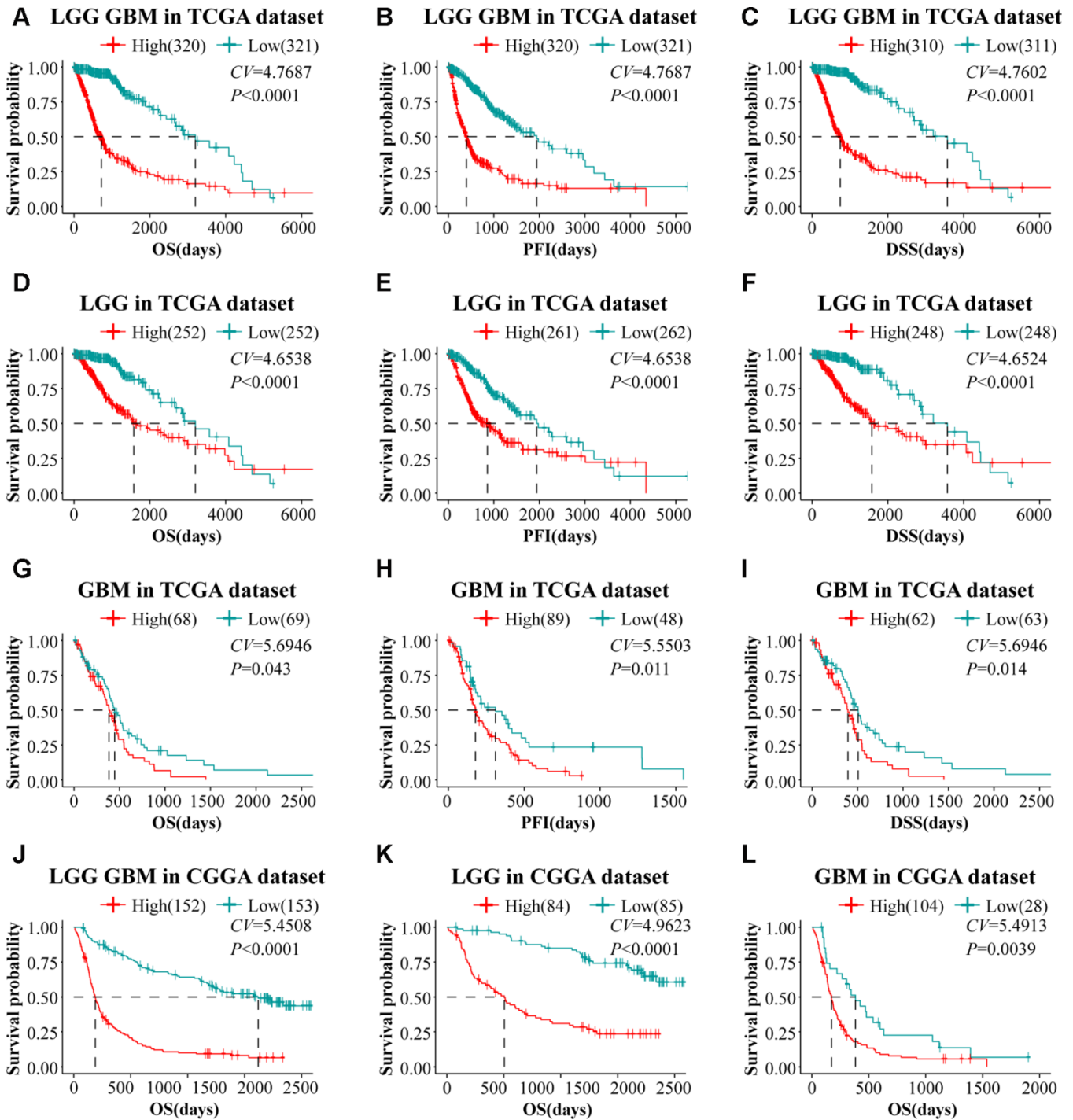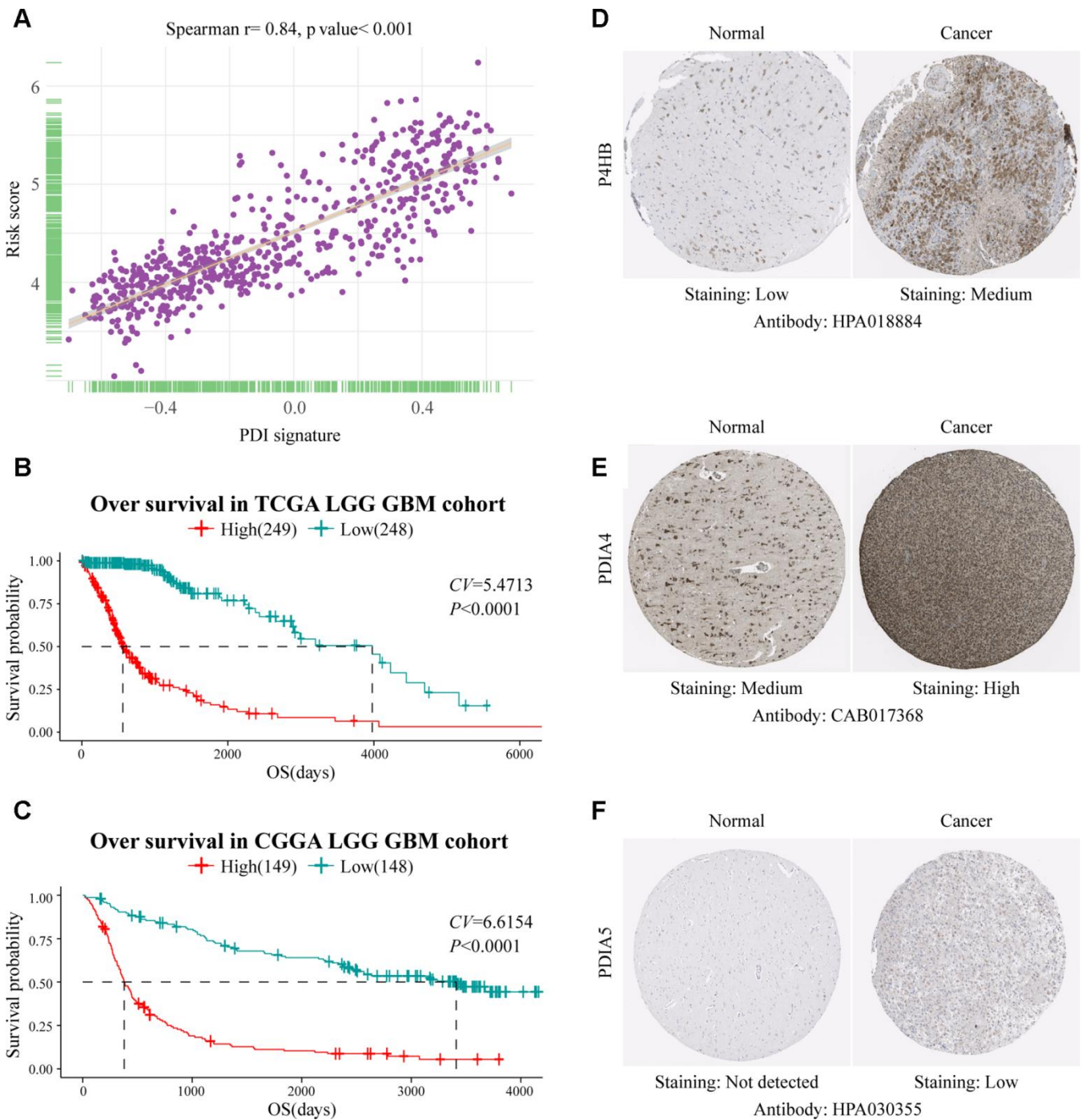
Supplementary Figure 4. The prognostic value of risk scores in patients with gliomas. Kaplan-Meier survival curves for the OS, PFI and DSS, according to the risk score values in LGGGBM (**A**–**C**), LGG (**D**–**F**), and GBM (**G**–**I**) samples downloaded from TCGA database. (**J**–**L**) The survival curves for the OS based on datasets from the CCGA database. TCGA database as training set and CGGA database as the validation set. CV, cut-off value used to divide patients into high and low groups.

Supplementary Figure 5. (**A**) Correlation between PDI signature and risk score. (**B**–**C**);Comparison of OS between two groups divided by the median value of the prognostic model (Low vs High). Representative immunohistochemical staining images of P4HB (**D**), PDIA4 (**E**), and PDIA5 (**F**), in normal brain tissues and high grade glioma tissues, which were downloaded from the Human Protein Atlas website (**www.proteinatlas.org**). TCGA database as training set and CGGA database as the validation set. CV, cut-off value used to divide patients into high and low group.

Supplementary Tables

Please browse Full Text version to see the data of Supplementary Tables 1

Supplementary Table 1. Univariate and multivariate Cox regression analysis of factors affecting overall survival of patients.

Supplementary Table 2. Clinical information of glioma patients from TCGA and CGGA database.

Clinicopathological features	TCGA	CGGA
	n (n%)	n (n%)
Number of patients	641 (100%)	319 (100%)
Subtype		
Proneural	229 (35.73%)	101 (31.66%)
Classical	79 (12.32%)	71 (22.26%)
Neural	108 (16.85%)	81 (25.39%)
Mesenchymal	90 (14.04%)	66 (20.69%)
NA	135 (21.06%)	0 (0.00%)
MGMT		
Methylation	460 (71.76%)	\
Unmethylation	150 (23.40%)	\
NA	31 (4.84%)	\
1p19q		
Codeletion	165 (25.74%)	67 (21.00%)
Noncodeletion	472 (73.63%)	245 (76.80%)
NA	4 (0.63%)	7 (2.20%)
IDH		
Mutation	417 (65.05%)	174 (54.55%)
Wildtype	217 (33.85%)	145 (45.45%)
NA	7 (1.10%)	0 (0.00%)
Gender		
Male	371 (57.88%)	198 (62.07%)
Female	270 (42.12%)	121 (37.93%)
Age		
<45	315 (49.14%)	187 (58.62%)
≥45	326 (50.86%)	132 (41.38%)
Grade		
WHO grade II	244 (38.07%)	102 (31.97%)
WHO grade III	259 (40.41%)	77 (24.14%)
WHO grade IV	137 (21.37%)	136 (42.63%)
NA	1 (0.15%)	4 (1.26%)
Cancer type		
LGG	504 (78.63%)	179 (56.11%)
GBM	137 (21.37%)	136 (42.63%)
NA	0 (0.00%)	4 (1.26%)